



1 **Periodic input of dust over the Eastern Carpathians during**  
2 **the Holocene linked with Saharan desertification and human**  
3 **impact**

4 Jack Longman<sup>1</sup>, Daniel Veres<sup>2</sup>, Vasile Ersek<sup>1</sup>, Ulrich Salzmann<sup>1</sup>, Katalin Hubay<sup>3</sup>, Marc  
5 Bormann<sup>4</sup>, Volker Wennrich<sup>5</sup>, Frank Schäbitz<sup>4</sup>

6 <sup>1</sup> Department of Geography, Northumbria University, Newcastle-Upon-Tyne, United Kingdom

7 <sup>2</sup> Romanian Academy, Institute of Speleology, Clinicilor 5, Cluj-Napoca, Romania

8 <sup>3</sup> Hungarian Academy of Science - Institute for Nuclear Research, Hertelendi Laboratory of Environmental  
9 Studies, H-4026 Debrecen, Bem ter 18/C, Hungary

10 <sup>4</sup> Institute of Geography Education, University of Cologne, 50931 Köln, Germany

11 <sup>5</sup> Institute of Geology and Mineralogy, University of Cologne, 50674 Köln, Germany

12

13 Correspondence to: Jack Longman (jack.longman@northumbria.ac.uk) and Daniel Veres  
14 (daniel.veres@ubbcluj.ro)

15

16 **Abstract.** Reconstructions of dust flux have been used to produce valuable global records of changes in  
17 atmospheric circulation and aridity. These studies have highlighted the importance of atmospheric dust in  
18 marine and terrestrial biogeochemistry and nutrient cycling. By investigating a 10,800-year long paleoclimate  
19 archive from the Eastern Carpathians (Romania) we present the first peat record of changing dust deposition  
20 over the Holocene for the Carpathian-Balkan region. Using qualitative (XRF core scanning) and quantitative  
21 (ICP-OES) measurements of lithogenic (Fe, K, Si, Ti) elements, we identify 11 periods of major dust deposition  
22 between: 9500-9100, 8400-8100, 7720-7250, 6350-6000, 5450-5050, 4130-3770, 3450-2850, 2100-1450, 800-  
23 620, and 60 cal yr BP to present. In addition, we used testate amoeba assemblages preserved within the peat to  
24 infer local palaeohydroclimate conditions. Our record highlights several discrepancies between eastern and  
25 western European dust depositional records, and the impact of highly complex hydrological regimes in the  
26 Carpathian region. After 6100 cal yr BP, we find that the geochemical indicators of dust flux become uncoupled  
27 from the local hydrology. This coincides with the appearance of millennial-scale cycles in the dust input and  
28 changes in geochemical composition of dust. We suggest this is indicative of a shift in dust provenance from  
29 local/regional (likely loess-related) to distal (Saharan) sources which coincide with the end of the African  
30 Humid Period and the onset of Saharan desertification.

31 **1 Introduction**

32 Atmospheric dust plays a major role in oceanic and lacustrine biogeochemistry and productivity (Jickells, 2005)  
33 by providing macronutrients to these systems (Mahowald et al., 2010). Furthermore, climatically dust plays a  
34 role in forcing precipitation (Ramanathan, 2001; Yoshioka et al., 2007) and in moderating incoming solar  
35 radiation. As such, reconstructions of past dust flux are an important tool to understand Holocene climate  
36 variability, biogeochemical cycles, and the planet's feedback to future changes in atmospheric dust loading.

37 The link between atmospheric circulation patterns and dust input has been studied intensively (Allan et al.,  
38 2013; Kylander et al., 2013; Marx et al., 2009; Le Roux et al., 2012) with clear evidence of climate variations  
39 linked with the dust cycle (Goudie and Middleton, 2006). Generally, dust is produced in arid zones (Grousset



40 and Biscaye, 2005) and may be transported thousands of miles before deposition (Grousset et al., 2003). In  
41 addition, dust input into the atmosphere can increase significantly during droughts (e.g. Miao et al., 2007;  
42 Notaro et al., 2015; Sharifi et al., 2015). As such, fluctuations in dust loading may be indicative of both regional  
43 drying and long-distance transport (Le Roux et al., 2012).

44 Hydroclimatic fluctuations had a significant effect on the development of civilisations throughout the Holocene  
45 (Brooks, 2006; deMenocal, 2001; Sharifi et al., 2015), especially on those which relied heavily on agriculture  
46 and pastoralism, as was the case in the Carpathian-Balkan region (Schumacher et al., 2016). To understand the  
47 impact hydroclimatic changes had on the population of an area of such importance to European history, high-  
48 resolution palaeoclimate and palaeohydrological records are needed. This is especially important in the  
49 Carpathian region, given the extensive loess cover in the area (Marković et al., 2015) - a fundamental factor in  
50 sustaining high agricultural production. Additionally, the sensitivity of loess to moisture availability and water  
51 stress during dry periods may turn this region and other surrounding loess belts into major dust sources (Kok et  
52 al., 2014; Rousseau et al., 2014; Sweeney and Mason, 2013). This is particularly true under semi-arid (Edri et  
53 al., 2016), or agriculturally-altered conditions (Korcz et al., 2009), as is the case with the major dust fields of  
54 Eastern Eurasia (Buggle et al., 2009; Smalley et al., 2011; Újvári et al., 2012). Thus, the dust influx into the  
55 Carpathian-Balkan region should be extremely sensitive to relatively small changes in precipitation rates. This  
56 hydroclimatic sensitivity is enhanced due to the fact that the Carpathians and the surrounding lowlands are  
57 located at a confluence of three major atmospheric systems; the North Atlantic, the Mediterranean and the  
58 Siberian High (Obrecht et al., 2016). Indeed, research appears to indicate the climate in Romania is controlled, at  
59 least in part, by North Atlantic Oscillation (NAO) fluctuations (Bojariu and Giorgi, 2005; Bojariu and Paliu,  
60 2001) but it is yet unclear how this relationship evolved in the past.

61 Multi-proxy and high resolution studies of palaeoenvironment in the region are still scarce, with most focusing  
62 on reconstructing past vegetation changes (e.g., Feurdean et al., 2012). More recently, testate amoeba  
63 (Schnitchen et al., 2006; Feurdean et al., 2015), pollen and diatoms (Magyari et al., 2009, 2013, Buczko et al.,  
64 2013), and macrofossils (Gałka et al., 2016) have been utilised to elucidate the history of hydroclimatic  
65 variability in the region. What is evident from these studies is the high inter-site variability, with clear  
66 disagreements on timing and extent of wet and dry periods within a relatively small spatial distribution (e.g.,  
67 two spatially close sites displaying differing precipitation trends as reported in Feurdean et al. (2008)). It is  
68 possible that this variability reflects only site-related (including chronological) uncertainties, or is an indicator of  
69 the impact of location at the contact of several climatic zones (Obrecht et al., 2016). To determine this, the impact  
70 of different modes of atmospheric (and moisture) circulation patterns and their imprint within paleoclimate  
71 archives must be investigated through better regional coverage following high-resolution multi-proxy  
72 approaches (e.g. Longman et al., in review.).

73 Our research provides a record of periodic dry and/or dusty periods in Eastern Europe as indicated by  
74 reconstructed dust input, using an ombrotrophic bog from the Romanian Carpathians (Fig.1). As the only source  
75 of clastic material deposited within ombrotrophic bogs is via atmospheric loading, such records have been used  
76 convincingly as archives of dust deposition over the Holocene in Western Europe and Australia (Allan et al.,  
77 2013; Kylander et al., 2013; Marx et al., 2009, 2010; Le Roux et al., 2012). To produce records of dust and/or  
78 hydroclimate variability, both inorganic (Allan et al., 2013; Ross-Barracough and Shoty, 2003; Shoty, 2002)



79 and organic (Booth et al., 2005; Lamentowicz et al., 2008; Morris et al., 2015; Swindles et al., 2010) proxies  
80 may be utilised (see Chambers et al. 2012 for a review).

81 Here we present the first record of dust input over the Carpathian Mountains, documenting changes in dust flux,  
82 source and intensity of deposition using the downcore lithogenic element concentrations from the Mohos  
83 ombrotrophic bog profile. The record covers 10,800 years of deposition over 9.5 m of peat, providing a much-  
84 needed high-resolution record for this region. Our research utilises both organic and inorganic proxies, with a  
85 high-resolution geochemical record of lithogenic elements (Ti, Si, and K), presented alongside the bog surface  
86 wetness as reconstructed using testate amoeba to understand dust source changes and the link between regional  
87 and extra regional hydroclimate variability and dust.

## 88 **2 Materials and Methods**

### 89 **2.1 Geographical Setting**

90 The Mohos peat bog (25°55' E; 46°05' N; 1050 m altitude, Figure 1) is located in the Eastern Carpathians,  
91 Romania, in the Ciomadul volcanic massif. The *Sphagnum*-dominated bog covers some 80 hectares, and  
92 occupies an infilled volcanic crater. There is no riverine inflow, which means that inorganic material deposited  
93 within the bog is predominantly derived via direct atmospheric transport. The climate is temperate continental,  
94 with average annual temperatures of 15°C and precipitation of 800 mm (Kristó, 1995). Surrounding vegetation  
95 is typical of this altitude in the Carpathians (Cristea, 1993), the bog being located at the upper limit of the beech  
96 forest, with spruce also found on surrounding slopes. Vegetation on the bog itself is diverse, with common  
97 occurrences of *Pinus sylvestris*, *Alnus glutinosa*, and *Betula pubescens*, alongside various *Salix* species (Pop,  
98 1960; Tanțău et al., 2003).

99 The Mohos crater is related to volcanic activity from the Ciomadul volcano, which last erupted roughly 29.6 cal  
100 kyr BP in the neighbouring younger crater currently occupied by the Lake St Ana (Harangi et al., 2010;  
101 Karátson et al., 2016; Magyari et al., 2014; Wulf et al., 2016). The surrounding geology is dominated by  
102 andesites and dacites, occasionally capped by pyroclastic deposits and a thick soil cover.

### 103 **2.2 Coring**

104 A Russian peat corer was used to recover a 950-cm long peat sequence from the middle part of Mohos bog. The  
105 material consists mainly of *Sphagnum* peat and lacustrine sediments in the lowermost part. Upon recovery, the  
106 material was transported to the laboratory, described, imaged, and subjected to further analyses.

### 107 **2.3 Sedimentological Parameters**

108 Loss on ignition (LOI) was performed on ~1g (exactly 1cm<sup>3</sup>) of wet peat, sampled at 2cm resolution. The peat  
109 was dried overnight at 105°C prior to ignition at 550°C for four hours. Weight loss after this combustion was  
110 used to calculate combusted organic material, followed by further combustion at 950°C for two hours to  
111 calculate total carbon content following carbonate removal (Heiri et al., 2001). The dry bulk density was  
112 determined from the known volume and the dry weight prior combustion.

### 113 **2.4 Micro-XRF and MSCL Core Scanning**

114 Non-destructive X-Ray fluorescence analysis was performed using an ITRAX core scanner (Croudace et al.,  
115 2006) at the University of Cologne (Institute of Mineralogy & Geology). The analytical resolution employed a  
116 2-mm step size and 20 s counting time using a Cr X-ray tube set to 30 kV and 30 mA (and including a Si-drift



117 chamber detector). The method allows for a wide range of elements to be analysed, from which we have  
 118 selected Ti, K, and Si for further interpretation. To allow for clearer viewing, all XRF data sets were smoothed  
 119 using a 10-point adjacent averaging. Due to the methodological nature of XRF core scanning, the data are  
 120 presented as counts per second (cps) and are therefore considered as semi-quantitative. Due to poor counting  
 121 statistics, any values below 50cps should be treated with caution. Alongside geochemical analyses, magnetic  
 122 susceptibility (MS) was determined in 0.5 cm steps using a multi scanner core logger (MSCL, Geotek Ltd.) at  
 123 the University of Cologne equipped with a Bartington MS2E spot-reading sensor.

#### 124 **2.5 ICP-OES**

125 To perform quantitative analysis of elements to allow inference of past dust flux, as well as to validate the  
 126 ITRAX data, ICP-OES analysis was carried out on 105 samples, at roughly 100-year resolution. These samples  
 127 were dried at 105°C overnight before homogenising using a pestle and mortar and then subjected to a mixed  
 128 acid (HNO<sub>3</sub>: HCl: HF) total digestion (adapted from Krachler et al., 2002), for 40 minutes in a MARS  
 129 accelerated reaction system. The solution was then analysed using a Perkin Elmer Optima 8000 ICP-OES  
 130 system at Northumbria University. To monitor a potential instrumental drift, internal standard (1ppm Sc) was  
 131 added to all samples, and analysed alongside Ti. In addition, two Certified Reference Materials (CRMs) were  
 132 digested and analysed throughout the runs (Montana soil 2711 and NIMT/UOE/FM/001). Recoveries for both  
 133 CRMs were good for Ti, with average values of 85% and 79% respectively. Blanks with negligible Ti  
 134 contamination were run alongside the samples and CRMs.

#### 135 **2.6 Calculating Dust Flux**

136 The dust flux delivered to an ombrotrophic bog via atmospheric loading may be calculated using the  
 137 concentration of a lithogenic element, such as Ti (Allan et al., 2013). Using the averaged occurrence of Ti in the  
 138 upper continental crust (UCC values from Wedepohl, 1995), the density of the peat as well as the peat  
 139 accumulation rate (PAR), the following formula may be used:

$$Dust\ Flux\ (g\ m^{-2}yr^{-1}) = \left( \frac{[Ti]_{sample}}{[Ti]_{UCC}} \right) \times density \times PAR \times 10000 (Eq. 1)$$

#### 140 **2.7 Palaeoecological indicators**

141 A total of 44 samples of roughly 1cm<sup>3</sup> each were sampled along the peat profile for testate amoeba analysis. The  
 142 bulk samples were disaggregated and sieved according to Booth et al. (2010), prior to mounting in water on  
 143 slides. Two tablets of Lycopodium spores of known value were added to allow for calculation of test density.  
 144 For each sample at least 150 tests were counted, with identification of taxa following Charman et al. (2000). For  
 145 interpretation, two methods of determining wet and dry local depositional environments based on changes in  
 146 testate amoeba assemblages were used. Firstly, a transfer function (Schnitchen et al., 2006) already applied to  
 147 Carpathian bogs was used to reconstruct past variations in the depth of the water table (DWT). Secondly, the  
 148 main taxa were grouped into their affinity to wet or dry conditions according to Charman et al. (2000) and  
 149 plotted as a function of percentage.

#### 150 **2.8 Chronology**

151 The age model for the Mohos peat record is based on 16 radiocarbon dates on bulk peat (collected over less than  
 152 1 cm depth interval per sample) consisting only of *Sphagnum* moss remains (Table 1). These analyses were  
 153 performed via EnvironMICADAS accelerator mass spectrometry (AMS) at the Hertelendi Laboratory of



154 Environmental Studies (HEKAL), Debrecen, Hungary using the methodology outlined in Molnár et al. (2013).  
155 The  $^{14}\text{C}$  ages were converted into calendar years using the IntCal13 calibration curve (Reimer et al., 2013) and  
156 an age-depth model (see Fig. 2) was generated using Bacon (Blaauw and Christen, 2011).

## 157 2.9 Spectral Analysis

158 Continuous Morlet wavelet transform was used to identify non-stationary cyclicities in the data (Grinsted et al.,  
159 2004; Torrence and Compo, 1998). For this analysis, the lithogenic elemental data from ITRAX measurements  
160 (Ti, K, Si and Fe) were interpolated to equal time steps of four years using a Gaussian window of 12 years.

## 161 3 Results

### 162 3.1 Age Model and Lithology

163 The Mohos peat profile is 950 cm long, and reaches the transition to the underlying basal limnic clay (Tanțău et  
164 al., 2003). Between 950-890 cm the record is composed of organic detritus (gyttja) deposited prior to the  
165 transition from a wetland into a bog. From 890 cm upwards, the core is primarily *Sphagnum*-dominated peat.  
166 The age-depth model indicates the Mohos peat record covers almost 10,800 years of deposition, with the  
167 uppermost layer (growing moss) of the peat dating to 2014. Thus, the resolution for ITRAX data average  
168  $\sim 5\text{yr/sample}$  and for ICP-OES is roughly  $100\text{ yr/sample}$ , respectively. The testate amoeba resolution is roughly  
169  $200\text{ yr/sample}$ . In the following, all quoted ages are in calibrated years before present (cal yr BP).

### 170 3.2 Dust indicators

#### 171 3.2.1 Ti, K, and Si

172 Similar trends for the lithogenic elements Ti, and Si, and the mobile element K, are visible in the record (Fig. 3),  
173 with 11 main zones of higher counts above typical background values present in all elements. These intervals  
174 are further discussed as reflecting major dust deposition events, and are referenced in the remainder of the text  
175 using the denotation D0-D10 (Fig. 3). We identify such events via the presence of a significant increase in one  
176 or more of these elements. The lithogenic, and therefore soil and rock derived Ti and Si have previously been  
177 used as proxies for dust input (e.g. Allan et al., 2013; Sharifi et al., 2015), whilst K covaries with Si ( $r^2=0.9945$ )  
178 and so controlling factors on their deposition must be nearly the same. For these elements, the periods with  
179 inferred non-dust deposition are characterised by values approaching the detection limit (150, 15 and 40 cps,  
180 respectively). A short period of very high values for all elements (10,000, 1300 and 8000 cps, respectively) is  
181 observed between 10,800-10,500 cal yr BP (not shown on diagram), reflecting the deposition of clastic  
182 sediments within the transition from lake to bog at the onset of the Holocene. Zones of elevated values (D0-D5),  
183 with average cps values roughly  $\text{Ti}=300$ ,  $\text{Si}=30$  and  $\text{K}=100$  and persisting for several centuries each, occur  
184 sporadically throughout the next 6000 years of the record, between 9500-9100, 8400-8100, 7720-7250, 6350-  
185 6000 and 5400-5050 cal yr BP (Fig. 3). Similarly long periods, but with much higher element counts ( $\text{Ti}=800$ ,  
186  $\text{Si}=60$  and  $\text{K}=200$  cps) occur between 4130-3770, 3450-2850 and 2100-1450 cal yr BP (D6-8). Two final, short  
187 (roughly 100-year duration) but relatively large peaks (D9-10) may be seen in the last 1000 years, between 800-  
188 620 cal yr BP (with values  $\text{Ti}=300$ ,  $\text{Si}=40$  and  $\text{K}=100$  cps) and 75 cal yr BP to present ( $\text{Ti}=300$ ,  $\text{Si}=80$  and  
189  $\text{K}=400$  cps, respectively).



### 190 3.2.2 Dust Flux

191 Using the quantitative ICP-OES values of Ti (in ppm), and equation 1, the dust flux can be calculated (Fig. 3).

192 The ICP-OES Ti record shows very good correlation with the Ti data derived through ITRAX analysis,  
193 indicating the reliability of the XRF core scanning method even for such highly organic sediments (as already  
194 suggested by Poto et al., 2014), and validating its usage as proxy for deriving dust flux (Fig. 3).

195 The Ti-derived dust flux for most the record is below  $1 \text{ g m}^{-2}\text{yr}^{-1}$ , but with seven periods of dust deposition  
196 clearly identifiable for the last 6350 years, and several smaller fluctuations prior to that (mainly visible in the  
197 elemental data). The main peaks are similar in their timing to the ITRAX Ti trend, with three large peaks (dust  
198 flux  $>1.5 \text{ g m}^{-2}\text{yr}^{-1}$ ) located between 5400-5050, 2100-1450 and 800-620 cal yr BP, respectively (Fig. 3).  
199 Smaller peaks are present (dust flux  $0.5\text{-}1 \text{ g m}^{-2}\text{yr}^{-1}$ ) at 6350-6000, 4150-3770, and 3500-2850 cal yr BP,  
200 respectively.

### 201 3.3 Density and Loss-on-Ignition (LOI)

202 Density values are relatively stable throughout the core, with all samples ranging between  $0.06\text{-}0.1 \text{ g/cm}^3$ . This  
203 trend is different from the organic matter values, which typically oscillate around 90-100% over the entire  
204 record. The very base of the record is however an exception, denoting the gradual transition from limnic clays to  
205 the peat reaching, with organic matter 80-90% between 10,800-10,000 cal yr BP. Very occasional intervals with  
206 lower organic matter content (roughly 85%) may be observed at 5400, 4100-3900, 3300-3200, 1900-1800 and  
207 900-800 cal yr BP, respectively (Fig. 4).

### 208 3.4 Magnetic Susceptibility

209 The trend in magnetic susceptibility indicates that the peat is diamagnetic with values ranging from 0 to  $-2.5 (10^{-5} \text{ SI})$ . Slight increases up to  $-1.5 (10^{-5} \text{ SI})$  may be observed 10,500-10,000, 7500-6500, and 2700-2450 cal yr BP.  
210  
211 The highest values are in the topmost section of the record, with a sharp increase after 50 cal yr BP (Fig. 4).

### 212 3.5 Testate Amoeba

213 Two methods of clarifying the paleoclimate signal derived through investigating testate amoeba assemblages  
214 have been used (Charman et al., 2000; Schnitchen et al., 2006), with both indicating similar hydroclimatic  
215 trends. Reconstructions of depth to water table (DWT) values indicate three main trends within the record. The  
216 first, encompasses the time period between 10,800-7000 cal yr BP, and is characterised by highly fluctuating  
217 values, with four very dry periods (DWT  $\sim 20 \text{ cm}$ ) at 10,800-10,200, 9000-8800, 8600-7600, and 7400-6600 cal  
218 yr BP interspersed by wetter (DWT  $15 \text{ cm}$ ) conditions (Fig. 4). After 7000 cal yr BP, values are much more  
219 stable, with DWT of  $15 \text{ cm}$  until the final zone, the last 100 years, where DWT rises to  $20 \text{ cm}$ . These fluctuations  
220 are in line with those seen in the wet/dry indicator species.

### 221 3.6 Wavelet Analysis

222 The wavelet analysis of K, Si and Ti show significant (above the 95% confidence threshold) periodicities  
223 between 1000-2000 years within the past 6000 years (Fig. 8). Prior to this, there appears to be no major cyclicity  
224 in the ITRAX data. Within periods which display raised ITRAX counts, shorter frequency (50-200 year) cycles  
225 are seen. These persist only for the period in which each element was enriched, particularly within the last 6000  
226 years.



## 227 4 Discussion

### 228 4.1 Peat ombrotrophy

229 The relative intensities of the lithogenic elements analysed via ITRAX covary throughout the record (Fig. 3),  
230 despite their varying post-depositional mobility (Francus et al., 2009; Kylander et al., 2011). For example, the  
231 largely immobile Ti shows a very high correlation with that of redox sensitive Fe ( $R^2 = 0.962$ ) and mobile K ( $R^2$   
232  $= 0.970$ ). This indicates the downcore distribution of these elements is mostly unaffected by post-depositional  
233 mobilisation via groundwater leaching and/or organic activity as documented in other studies (e.g. Novak et al.,  
234 2011; Rothwell et al., 2010). This, alongside the low clastic content (average organic matter of 91%), low  
235 density and domination of *Sphagnum* organic detritus, indicates the ombrotrophic nature of Mohos bog  
236 throughout time and validate the use of this record to reconstruct dust fluxes for the last ca. 10,000 years (Fig.  
237 3).

### 238 4.2 The Dust Record

239 The record of inferred lithogenic (dust) input as indicated by Ti, K and Si documents 11 well-constrained  
240 periods of major and abrupt dust deposition (denoted D0-D10), with further small, short-term fluctuations (Fig.  
241 3). The dust influx onto the Mohos peat was accompanied by decreases in organic matter (OM) as indicated  
242 from the LOI profile, and higher density values (Fig. 4), particularly over the intervals covered by events D5-  
243 D10. The major dust deposition events last from a few decades to hundreds of years (Fig. 3).

244 Firstly, it is noteworthy that five of the identified dust depositional events correlate to periods of Rapid Climate  
245 Change (RCC) as outlined by Mayewski et al. (2004) from the Greenland GISP2 record (Fig. 5). However,  
246 despite apparent hemispheric-scale influences, the dust events identified within Mohos record have little  
247 correlation to reconstructed European paleoclimate changes during Holocene. For example, the dust event  
248 between 3000-2700 cal yr BP falls within a cold period (Wanner et al., 2011). In contrast, the event between  
249 860-650 cal yr BP is within the Medieval Climate Anomaly, a period of generally higher European temperatures  
250 (Mann et al., 2009) but also one of intense human impact on the environment thorough deforestation and  
251 agriculture (Arnaud et al., 2016; Kaplan et al., 2009). This indicates the dust depositional events are a result of a  
252 complex interplay of environmental conditions in the dust source areas, rather than simply reflecting warm or  
253 cold, or even wet or dry periods.

254 In addition to the North Atlantic, the impact of both the Mediterranean and the intertropical convergence zone  
255 (ITCZ) atmospheric systems influencing the Mohos dust record are apparent, including major climate changes  
256 in North Africa. D4 for example occurs within the chronological span of the 5900 cal yr BP event, a major  
257 cooling and drying period (Bond et al., 2001; Cremaschi and Zerboni, 2009; Shanahan et al., 2015). Increased  
258 dust influx is also recorded around 5300 cal BP (D5, Fig. 3) which roughly correlates with the end of the  
259 African Humid Period and onset of Saharan desertification (deMenocal et al., 2000). The lack of dust flux  
260 perturbations prior to 6100 yr BP, and their prevalence thereafter at Mohos appear to indicate a major shift in  
261 the controls of dust production and deposition at this time. The desertification of the Sahara around this time  
262 was the largest change in dust production in the northern hemisphere (see McGee et al., 2013; deMenocal et al.,  
263 2000).



264 Within our record, this initial dust flux increase was followed by a period of reduced dust loading, prior to a  
265 rapid, and apparently major (highest dust flux values in the record prior to the most recent two millennia) event  
266 at 5400-5000 cal yr BP. Regionally, Saharan dust in Atlantic marine cores strongly increased at this time, with a  
267 140% rise roughly at 5500 cal yr BP (Adkins et al., 2006) and another rise by a factor of 5 by 4900 cal yr BP  
268 (McGee et al., 2013). Furthermore, evidence from marine cores across the Mediterranean indicate decreasing  
269 Nile output and increasing dust fluxes into the Eastern Mediterranean at this time (Box et al., 2011; Revel et al.,  
270 2010). The correlation of these data to the Mohos record appears indicative of the region-wide impact of North  
271 African desertification. It is noteworthy, as seen in Fig. 5, that the release of dust from the Sahara correlates well  
272 with increasing frequency and intensity of dust fluxes at Mohos after 6000 cal yr BP, with all major (dust flux  
273  $>0.5 \text{ g m}^{-2}\text{yr}^{-1}$ ) Ti-derived dust flux peaks occurring after this time (Fig. 3). This period is the first indication of  
274 the impact the Mediterranean climate and movement of the ITCZ has had on the Carpathian-Balkan region (as  
275 simulated by Egerer et al. (2016) and Boos and Korty (2016)). Indeed, intermittent intrusions of Saharan dust  
276 over the Carpathian area have been well documented both through direct observations (Labzovskii et al., 2014;  
277 Varga et al., 2013), and through provenance studies of past Saharan dust contribution within interglacial soils in  
278 the region (Varga et al., 2016).

279 In addition to Saharan desertification, it is likely that early agriculture in the Carpathian-Balkan region has  
280 contributed towards the increase in dust flux values at this time. It is known that advanced agriculture-based  
281 societies inhabited the Carpathian area in the mid-Holocene (Carozza et al., 2012), with evidence of farming  
282 seen in a number of pollen records (see Schumacher et al., 2016 for a compilation), including in Mohos itself at  
283 the end of the Chalcolithic period (Tanțău et al., 2003). Since agriculture and soil erosion may be linked, it is  
284 possible events D4 and D5 could also reflect to some extent dust input related to land disturbance by human  
285 activities, on a regional scale. However, such evidence for agriculture, particularly in the proximity of Mohos is  
286 limited to a few *Plantago* and cereal pollen (Tanțău et al., 2003), whilst the majority of pollen studies in  
287 Romania at this time indicate no significant agricultural indicators (e.g. Magyari et al., 2010; Schumacher et al.,  
288 2016; Tanțău et al., 2014). As such, it seems unlikely agricultural activity is behind such a large change in the  
289 dust deposition record from Mohos.

#### 290 **4.3 Geochemical evidence for a dust provenance shift at 6100-6000 cal yr BP?**

291 To better understand the nature of the shift in dust flux after 6100-6000 cal yr BP, a simple approach to  
292 disentangling the geochemical makeup of the reconstructed dust load is discussed below. Figure 6 displays the  
293 clustering of the lithogenic elements Ti and K (and Si, due to the similarity in the Si and K records) during dust  
294 events D0-D10. The data appear to show three main types of dust (and presumably sources), one with high  
295 values for both Ti and K (Type 1), one with relatively high values for K (Type 2), and one with relatively high  
296 Ti compared to K (Type 3). The values for Ti-K correlation, average Ti and average K (in cps) are listed in  
297 Table 2. Generally, the periods of no enrichment, and low K and Ti, do not show any correlation, indicative of  
298 natural background and instrumental detection limits.

299 Type 1 deposition occurs only in D10, and is characterised by Ti-K gradient of nearly 1, indicating similar  
300 values for both elements throughout the period, and a dust rich in both K and Ti. Type 2 deposition occurs in  
301 several the dust events, particularly in D1-2, D4-5, and D7 (Fig. 8). The K enrichment which characterises these  
302 events is, evidenced by the Ti-K gradients  $<1$  and low (even negative in the case of D2) correlations between the





303 two elements. Finally, Type 3 events (D3, D6, and D8-9) are characterised by an increased Ti-K gradient,  
304 generally, around 0.2. The average Ti values during these events and the Ti-derived dust flux, are generally  
305 highest in these periods (Table 2). These groupings would indicate similar dust sources within grouped events,  
306 and may aid in identifying provenance.

307 Type 2 events typically occur in the older part of the record, except D7 (3400-3000 cal yr BP, Fig.8). Such  
308 events are not visible in the Ti-derived dust flux values, indicative of the reduced impact of Ti-bearing dust  
309 particles deposited within the corresponding periods. The local rocks consist of K-rich dacites and pyroclastics  
310 (Szakács et al., 2015), with relatively low Ti concentrations and enriched in K (Vinkler et al., 2007). Therefore,  
311 the likely source of particulates deposited during these dust events is local or regional, with nearby (or even  
312 distal) loess and loess-like deposits as another potential source, since loess sediments in south-eastern Europe  
313 are generally not enriched in Ti (Bugge et al., 2008).

314 Type 3 events, conversely, appear Ti-enriched (Fig.8), with contribution from a source away from the low-Ti  
315 dust of south-eastern European loess fields. These events typically occur after 6100 cal yr BP (Fig. 3). With the  
316 periodic influence of the Mediterranean air masses in the region ((Apostol, 2008; Bojariu and Paliu, 2001)),  
317 Saharan dust must be considered as a potential source area, since it appears to play a major role in dust input  
318 into Europe today (e.g. Athanasopoulou et al., 2016). Geochemically, Saharan dust is typically Ti-enriched  
319 (Nicolás et al., 2008). In particular, the Bodélé depression, the single-largest dust source in the Sahara, exhibits  
320 extremely high Ti/Al and Ti enrichment (Bristow et al., 2010; Moreno et al., 2006). The Ti enrichment does not  
321 show any regional trends, and so it is no use for determining exact source areas within the Sahara (Scheuven et  
322 al., 2013), but the presence of Ti-enriched dust appears to reflect a signal of Saharan influence. Consequently,  
323 events of Type 3 may be considered to reflect, at least to a large extent, contribution of Saharan dust. Finally,  
324 the single Type 1 event may be attributable to a mixing of sources, both local (resulting in high K) and distal  
325 (resulting in high Ti), evidence for Saharan input and local soil erosion/deflation.

326 Previous work has indicated the input of Saharan dust in Eastern Europe, with evidence of such a source seen in  
327 Carpathian loess (Újvári et al., 2012; Varga et al., 2013) and soil-forming dust (Varga et al., 2016).  
328 Additionally, recent atmospheric satellite imagery has further confirmed the extent of Saharan dust outbreaks  
329 and depositional events over central-eastern Europe (Varga et al., 2013). However, the lack of long-term dust  
330 reconstructions in the region has so far precluded understanding of changing dust sources over the Holocene.

331 Previous studies across Europe indicate the complex input of dust from various sources over the mid-to-late  
332 Holocene (e.g., Veron et al., 2014), but pertinently to our findings at Mohos, many examples exhibit a major  
333 shift in dust sources at roughly 5000-7000 cal yr BP. In Belgium, Nd isotopes indicate a local source of dust  
334 prior to input of European loess and Saharan dust after 6500 cal yr BP (Allan et al., 2013). This is echoed by  
335 data from Le Roux et al. (2012) that indicate a major shift in the Nd isotopic composition at 6000 cal yr BP,  
336 moving from a local to a mixed source, but with clear Saharan overprinting. The transition identified within the  
337 Mohos dust record at 6100-6000 cal yr BP, therefore, appears to echo the appearance of a Saharan dust element  
338 within other European bog-based dust reconstructions. However, it appears that input of Saharan dust was not  
339 limited to the onset of North Africa desertification, as indicated by input of likely Saharan derived dust within



340 Mohos event D3 already by 7800-7200 cal yr BP. Further, even after 6100 cal yr BP, local sources still played a  
341 significant role, with D7 showing clear local or regional (e.g., loess-derived) signal.

342 D10 is interesting in that it appears to indicate even more K-rich dust sources. These values are similar in  
343 compositional gradient to the lake sediment deposited prior to the onset of peat formation in the early Holocene  
344 (Gradient of lake sediment samples (Average of samples pre-10,500 cal yr BP) = 0.7429, D10= 1.0637). Since  
345 the surrounding dacites and pyroclastics are K-rich (Vinkler et al., 2007), and the natural signal of erosion into  
346 the lake occurs prior to peat formation, it is reasonable to assume this period is indicative of local slope erosion.  
347 This is potentially due to the decline of the local forest and agricultural intensification, identified in the most  
348 recent sections of the Mohos pollen record (Tanțău et al., 2003). It is sensible to assume the local deforestation  
349 (visible around the Mohos bog as meadows for hay harvesting) has caused local soil erosion and increased dust  
350 production from very proximal sources (Mulitza et al., 2010). This is a clear sign of the persistent human impact  
351 at local to regional scale at the time (Giosan et al., 2012; Schumacher et al., 2016) that is also mirrored in the  
352 nearby Lake St Ana record (Magyari et al., 2009). As indicated by regional studies (e.g., Labzovskii et al., 2014;  
353 Varga et al., 2013; Vukmirović et al., 2004) high levels of Ti indicate Saharan input does not cease through this  
354 period, but that it is matched by high-K local sources. The apparent higher water table of the Mohos bog as  
355 implied by the TA record and the increased Ti contents indicative rather point towards an increasing Saharan  
356 influence rather than a major local dust source.

#### 357 **4.4 Correlation to other European dust records**

358 Comparison to similar dust records from peat cores in Western Europe (Allan et al., 2013; Le Roux et al., 2012),  
359 and Atlantic margin sediments (McGee et al., 2013) reveals some interesting trends visible in all these records  
360 (Fig. 5), indicating comparable continent-wide controls on past dust flux. Specifically, the major dust event as  
361 seen at 5400-5000 cal yr BP in Mohos, and subsequent increase in number and intensity of dust events is  
362 comparable with an intensification of dust deposition over Europe after 6000 cal yr BP (Le Roux et al., 2012),  
363 with concurrent increases in dust flux in the Mid-Holocene documented in Belgium (Allan et al., 2013). The  
364 authors suggest a cool period (Wanner et al., 2011) as the cause of this dust increase. In addition to the  
365 reconstructed cool environments in Western Europe, this period is characterised by increased dust production in  
366 the Sahara (McGee et al., 2013), which is also likely to have played a role in the increasing dust flux over  
367 Europe. After 5000 cal yr BP, it appears Mohos and central-western European records show a more concurrent  
368 trend, with comparable dust peaks in the Swiss record (Le Roux et al., 2012) between 4100-3800, 3600-3050,  
369 850-600 and 75 cal yr BP also present in Mohos, and a similar dust peak at 3200-2800 cal yr BP identified in  
370 another bog record from Bohemia (Veron et al., 2014).

371 Despite some similarities between the records, there is also significant variability, highlighting the difference  
372 between climatic controls in western and central Europe and those in south-eastern Europe. The disconnection  
373 between Mohos and other records is particularly clear for the early Holocene, with large dust flux peaks  
374 identified in Switzerland between 9000-8400 cal yr BP and 7500-7400 cal yr BP, when there is little evidence of  
375 dust input into Mohos. This discrepancy could be indicative of the east-west (Davis et al., 2003; Mauri et al.,  
376 2015; Roberts et al., 2012) and north-south (Magny et al., 2013) hydroclimatic gradients in Europe throughout  
377 the Holocene. As other studies indicate, south-eastern Europe was mostly disconnected (in terms of both  
378 precipitation and temperature) from the rest of Europe in the early-Mid Holocene (Davis et al., 2003; Drăgușin



379 et al., 2014), clearly indicated by the trend in the Mohos dust record. Since the Sahara had not undergone  
380 significant desertification by this time, no clear correlation with western records may be made, hinting at more  
381 local source for the earliest five dust events identified within the Mohos record (Fig. 3). In addition, the dust  
382 events occurring during the early to mid-Holocene, which are not present in the Ti-derived dust record at  
383 Mohos, are more likely related to local fluctuations in moisture availability, and Si and K rich soil dust.

#### 384 4.5 Palaeoecological Proxy Record

385 To further investigate the difference between local and regional palaeoclimate signals within Mohos, and to  
386 reconstruct the local hydroclimate conditions throughout the record, we use the fossil assemblages of testate  
387 amoeba (TA). These data, alongside comparisons to existing Carpathian-Balkan and Mediterranean  
388 hydroclimate reconstructions (Fig.7), may be used to further investigate the theory of a distal (most likely  
389 Saharan) source for dust after 6100 cal yr BP. The earliest section in the TA record (10,800-6400 cal yr BP) is  
390 characterised by fluctuating dry/wet periods, indicative of large shifts in the local hydroclimatic environment  
391 (Fig. 4). The earliest identified dry period (10,800-10,000 cal yr BP) is linked to the shift away from a lacustrine  
392 to a palustrine environment as a result of local drying. Three subsequent dry periods may be identified in the TA  
393 record 9300-8800, 8500-8100, and 7800-7000 cal yr BP, all of which are also identifiable in the geochemical  
394 dust record (D1-D3) via trends in K and Si. Between 10,200-7450 cal yr BP, dust flux at Mohos was low. Dust  
395 events during this time are mainly present in the K and Si records (Fig. 3), or in OM and density parameters  
396 (Fig. 4).

397 The first period of elevated dust proxies at roughly 10,300 cal yr BP (D0) correlates well with the 10,200 cal yr  
398 BP oscillation (Rasmussen et al., 2007), previously linked to a drop in water levels at nearby Sf Ana Lake  
399 (Korponai et al., 2011; Magyari et al., 2012, 2014). High *Diffflugia pulex* and *Trigonopyxis arcuata* values during  
400 D1 as indicator taxa for dry conditions (Allan et al., 2013; Charman et al., 2000) appear to confirm local drying,  
401 observed across much of the Mediterranean (Berger et al., 2016; Buczkó et al., 2013; Magyari et al., 2013, Fig.  
402 7). The D2 and D3 events may also be observed in both the TA record and the geochemical dust record, with D2  
403 attributable to the 8200 cal yr BP event (Bond et al., 2001), a paleoclimatic event already identified in other  
404 local hydroclimate reconstructions (Buczkó et al., 2013; Magyari et al., 2013; Schnitchen et al., 2006). The  
405 transition to the next wet period at 8000 cal yr BP also mirrors the dust record, with a deeper water table  
406 occurring during the dust-free conditions between D2 and D3. This is prior to the bog undergoing dry conditions  
407 between 7800-7000 cal yr BP, roughly in line with D3, drying which has previously been observed in Romania  
408 (Galka et al., 2016; Magyari et al., 2009, Fig 7). Due to the covariance between geochemical and  
409 paleoecological proxies at this time, and the correlation to other local reconstructions, the early Holocene  
410 section of the record indicates a close linkage of local hydroclimate and dust input. These dust events, therefore,  
411 are likely the signal of remobilised material (Edri et al., 2016), from proximal or distal sources (including  
412 perhaps from loess-derived sediments, at the foot of Ciomadul volcano) as the climate locally appears to become  
413 more arid.

414 Between 6600-1200 cal yr BP, the TA indicate a shift to prolonged wet conditions, with only minor fluctuations  
415 and no clear correlation to the geochemically-derived dust record, and so the dust events appear unrelated to  
416 local drying within this time period (Fig. 7). This is indicative of a decoupling of the dust record from local



417 climate reconstructions, with dry phases common throughout the Mid-Late Holocene in other Romanian sites  
418 (e.g., Magyari et al., 2009; Schnitchen et al., 2006, Fig 7), and a distal dust source.

419 In the last millennium, there are two major dust events, with the first, D9, occurring between 850-650 cal yr BP.  
420 This episode falls within the late Medieval Warm Period, and could be related to human activity in the local  
421 area, as pollen from the Mohos bog indicates strong evidence for agriculture at roughly the same time (Tanțău et  
422 al., 2003). This may be seen in the intensity of the dust deposition at this time (dust flux  $>3 \text{ g m}^{-2}\text{yr}^{-1}$ ). D10,  
423 from 75 cal yr BP to present is certainly linked to such human influences, with the TA record echoing local  
424 studies, which display anthropogenically-altered conditions and intensive agriculture (Buczko et al., 2013;  
425 Diaconu et al., 2016; Giosan et al., 2012; Magyari et al., 2009, 2013; Morellón et al., 2016; Schnitchen et al.,  
426 2006, Fig. 7). This appears to validate the geochemical approach used earlier, as intensive farming is likely to  
427 result in local dust mobilisation, with K-rich dust present at this time. This does not preclude Saharan input,  
428 however, as the dust is also Ti-rich.

#### 429 **4.6 Periodicity**

430 To further understand the nature of the reconstructed dust events, cyclicity within the geochemical record was  
431 investigated using wavelet analysis (Fig. 8). The main elements of interest (Ti, Si and K) have no apparent  
432 cyclicity in the first half of the record (10,800-6000 cal yr BP), whilst the last 6000 years display clear  
433 centennial and millennial-scale cycles. A number of other studies have identified cyclicity shifts at this time  
434 (Fletcher et al., 2013; Jiménez-Espejo et al., 2014; Morley et al., 2014), related to North Atlantic variability, but  
435 so far mainly in western Mediterranean records. From 6000 cal yr BP onwards, the geochemical record at  
436 Mohos preserves two main cyclicities; one at ~1200-2000 years and the second at ~ 600-800 years (Fig. 8). A  
437 715-775 year cycle has been determined as a harmonic of Bond event-related dry periods, present in other  
438 Northern hemisphere records (Springer et al., 2008) and in central Africa (Russell et al., 2003). The 1200-2000  
439 years cycle, in contrast, is within the envelope of a 1750 year cycle observed within the western Mediterranean,  
440 in pollen (Fletcher et al., 2013) and Saharan dust (Debret et al., 2007; Jiménez-Espejo et al., 2014), which is  
441 attributed to changes in North Atlantic circulation.

442 Within the dust deposition events (Fig. 3), there is an overprinting of high-frequency cyclicity in the Ti record,  
443 especially within the last 5000 years (Fig. 8). These are particularly clear at 4200, 3400 and 1800 cal yr BP, but  
444 lower-confidence cyclicities may be seen in most dust deposition events. These are generally 100-200 years in  
445 length, and only last the extent of the dust outbreak. Cycles with lower than 140-year periodicities are possibly  
446 reflecting mainly background noise (Turner et al., 2016), but those longer in duration may be indicative of  
447 climatically forced fluctuations within drought events affecting the dust source areas. This suggests the  
448 reconstructed dust deposition events based on the Mohos record were not characterised by constant deposition  
449 of dust, but by periodic dust pulses. These short cycles could reflect solar forcing, with comparable 200-year  
450 cycles observed in humification profiles from peats (Swindles et al., 2012), sediments in the Baltic Sea (Yu,  
451 2003), Pacific Ocean (Poore et al., 2004), and in North American peatland isotope records (Nichols and Huang,  
452 2012). In many cases, such cycles have been linked to lower solar activity periods, low temperatures and  
453 increased precipitation oscillations, related to the De Vries/Suess 200 year cycle (Lüdecke et al., 2015). In the  
454 case of Mohos, these fluctuations have manifested themselves as shifts in dust deposition, and indicate the  
455 persistent effect solar dynamics has on all facets of climate system.



## 456 5 Conclusions

- 457 • The first record of Holocene drought and dust input in a bog from Eastern Europe documents eleven  
458 periods of high dust: 10,500-10,400, 9500-9100, 8400-8100, 7720-7250, 6150-5900, 5450-5050, 4130-  
459 3770, 3450-2850, 2100-1450, 800-620 and 60 cal yr BP to present.
- 460 • A major intensification in the number, and severity (as indicated by dust flux values) of dust events is  
461 observed after 6100 cal yr BP. Prior to this, dust flux was low, indicative of the local nature of the dust  
462 events recorded, and echoed by the testate amoeba assemblages, which displayed coeval drying of the  
463 bog surface and small (compare to the periods post 6100 cal yr BP) dust input. Thus, the dust record of  
464 the early to mid-Holocene may be more indicative of local-scale drought conditions.
- 465 • The timing of the major shift at 6100 cal yr BP is possibly related to the end of the African Humid  
466 Period, and the establishment of the Sahara Desert, pointing to significantly greater Saharan input  
467 within the regional dust loading after this time. This is corroborated by changes in cyclicity attributable  
468 to Saharan dust outbreaks, and a shift toward Ti-rich dust (a signal of Saharan rock and sediment)  
469 deposited onto the Mohos peat. Our data is the first such indication of the impact Saharan dust has had  
470 across Eastern Europe, in line with enhanced deposition of dust across the Mediterranean region. A  
471 tentative dust provenance analysis based on a simple geochemical approach to disentangle the  
472 composition of the dust has been applied to confirm this, with three main types of deposition  
473 documented, indicating the interplay between local/regional (mainly loess-derived) and Saharan dust  
474 sources over the Holocene.
- 475 • The most recent dust event, between 75 cal yr BP and today is geochemically indicative mainly of local  
476 erosion. This may be linked to the increasing human impact through deforestation, agriculture and  
477 recently tourism, and associated soil erosion, indicating a shift in the controls on drought and dust in  
478 the region.

479 **Author contribution.** J. Longman, D.Verés, V.Ersek and U.Salzmann designed the research, interpreted the  
480 results and wrote the paper. D.Verés, M.Bormann and F. Schabitz performed the fieldwork. J.Longman  
481 performed the ICP-OES, testate amoeba and statistical analysis. V.Ersek performed the wavelet analysis.  
482 M.Bormann, F.Schabitz and V.Wennrich performed the ITRAX and MSCL analysis. K.Hubay performed the <sup>14</sup>C  
483 dating. All authors approved the content of the paper.

484 **Competing interests.** The authors declare that they have no conflict of interest

485 **Acknowledgements.** We would like to thank Northumbria University for J.Longman's studentship. This is a  
486 contribution to the project PN-II-ID-PCE-2012-4-0530 "Millennial-scale geochemical records of anthropogenic  
487 impact and natural climate change in the Romanian Carpathians" and to the CRC806 "Our way to Europe"  
488 hosted at University of Cologne, Bonn & Aachen (subproject B2) granted by the DFG (German Research  
489 Foundation).

## 490 References

491 Adkins, J., DeMenocal, P. and Eshel, G.: The "African humid period" and the record of marine upwelling from  
492 excess 230 Th in Ocean Drilling Program Hole 658C, *Paleoceanography*, 21(4), 1–14,  
493 doi:10.1029/2005PA001200, 2006.



- 494 Allan, M., Le Roux, G., Piotrowska, N., Beghin, J., Javaux, E., Court-Picon, M., Mattielli, N., Verheyden, S.  
495 and Fagel, N.: Mid-and late Holocene dust deposition in western Europe: the Misten peat bog (Hautes Fagnes –  
496 Belgium), *Clim. Past*, 9, 2285–2298, doi:10.5194/cp-9-2285-2013, 2013.
- 497 Apostol, L.: The Mediterranean cyclones: the role in ensuring water resources and their potential of climatic  
498 risk, in the east of Romania, *Present Environ. Sustain. Dev.*, 2, 143–163, 2008.
- 499 Arnaud, F., Poulenc, J., Giguët-Covex, C., Wilhelm, B., Révillon, S., Jenny, J.-P., Revel, M., Enters, D.,  
500 Bajard, M., Fouinat, L., Doyen, E., Simonneau, A., Pignol, C., Chapron, E., Vannière, B. and Sabatier, P.:  
501 Erosion under climate and human pressures: An alpine lake sediment perspective, *Quat. Sci. Rev.*, 152, 1–18,  
502 doi:10.1016/j.quascirev.2016.09.018, 2016.
- 503 Athanasopoulou, E., Protonotariou, A., Papangelis, G., Tombrou, M., Mihalopoulos, N. and Gerasopoulos, E.:  
504 Long-range transport of Saharan dust and chemical transformations over the Eastern Mediterranean, *Atmos.*  
505 *Environ.*, 140, 592–604, doi:10.1016/j.atmosenv.2016.06.041, 2016.
- 506 Berger, J. F., Lespez, L., Kuzucuoglu, C., Glais, A., Hourani, F., Barra, A. and Guilaine, J.: Interactions between  
507 climate change and human activities during the Early to Mid Holocene in the East Mediterranean basins, *Clim.*  
508 *Past Discuss.*, (February), 1–42, doi:10.5194/cp-2016-4, 2016.
- 509 Blaauw, M. and Christen, J. A.: Flexible paleoclimate age-depth models using an autoregressive gamma  
510 process, *Bayesian Anal.*, 6(3), 457–474, doi:10.1214/ba/1339616472, 2011.
- 511 Bojariu, R. and Giorgi, F.: The North Atlantic Oscillation signal in a regional climate simulation for the  
512 European region, *Tellus*, 57A(4), 641–653, doi:10.1111/j.1600-0870.2005.00122.x, 2005.
- 513 Bojariu, R. and Paliu, D.-M.: North Atlantic Oscillation Projection on Romanian Climate Fluctuations in the  
514 Cold Season, *Detect. Model. Reg. Clim. Chang. Assoc. Impacts*, 2001.
- 515 Bond, G., Kromer, B., Beer, J., Muscheler, R., Evans, M. N., Showers, W., Hoffmann, S., Lotti-Bond, R.,  
516 Hajdas, I. and Bonani, G.: Persistent solar influence on North Atlantic climate during the Holocene., *Science*,  
517 294(5549), 2130–2136, doi:10.1126/science.1065680, 2001.
- 518 Booth, R. K., Jackson, S. T., Forman, S. L., Kutzbach, J. E., Bettis, E. a., Kreig, J. and Wright, D. K.: A severe  
519 centennial-scale drought in midcontinental North America 4200 years ago and apparent global linkages, *The*  
520 *Holocene*, 15, 321–328, doi:10.1191/0959683605hl825ft, 2005.
- 521 Booth, R. K., Lamentowicz, M. and Charman, D. J.: Preparation and analysis of testate amoebae in peatland  
522 palaeoenvironmental studies, *Mires Peat*, 7(2), 1–7, 2010.
- 523 Box, M. R., Krom, M. D., Cliff, R. A., Bar-Matthews, M., Almogi-Labin, A., Ayalon, A. and Paterne, M.:  
524 Response of the Nile and its catchment to millennial-scale climatic change since the LGM from Sr isotopes and  
525 major elements of East Mediterranean sediments, *Quat. Sci. Rev.*, 30(3), 431–442,  
526 doi:10.1016/j.quascirev.2010.12.005, 2011.
- 527 Bristow, C. S., Hudson-Edwards, K. A. and Chappell, A.: Fertilizing the Amazon and equatorial Atlantic with  
528 West African dust, *Geophys. Res. Lett.*, 37(14), n/a-n/a, doi:10.1029/2010GL043486, 2010.
- 529 Brooks, N.: Cultural responses to aridity in the Middle Holocene and increased social complexity, *Quat. Int.*,  
530 151(1), 29–49, doi:10.1016/j.quaint.2006.01.013, 2006.
- 531 Buczkó, K., Magyari, E. K., Braun, M. and Bálint, M.: Diatom-inferred lateglacial and Holocene climatic  
532 variability in the South Carpathian Mountains (Romania), *Quat. Int.*, 293, 123–135,  
533 doi:10.1016/j.quaint.2012.04.042, 2013.
- 534 Buggle, B., Glaser, B., Zöller, L., Hambach, U., Marković, S., Glaser, I. and Gerasimenko, N.: Geochemical  
535 characterization and origin of Southeastern and Eastern European loesses (Serbia, Romania, Ukraine), *Quat. Sci.*  
536 *Rev.*, 27(9), 1058–1075, doi:10.1016/j.quascirev.2008.01.018, 2008.



- 537 Buggle, B., Hambach, U., Glaser, B., Gerasimenko, N., Marković, S., Glaser, I. and Zöller, L.: Stratigraphy, and  
 538 spatial and temporal paleoclimatic trends in Southeastern/Eastern European loess-paleosol sequences, *Quat. Int.*,  
 539 196(1–2), 86–106, doi:10.1016/j.quaint.2008.07.013, 2009.
- 540 Carozza, J.-M., Micu, C., Mihail, F. and Carozza, L.: Landscape change and archaeological settlements in the  
 541 lower Danube valley and delta from early Neolithic to Chalcolithic time: A review, *Quat. Int.*, 261, 21–31,  
 542 doi:10.1016/j.quaint.2010.07.017, 2012.
- 543 Chambers, F. M., Booth, R. K., De Vleeschouwer, F., Lamentowicz, M., Le Roux, G., Mauquoy, D., Nichols, J.  
 544 E. and van Geel, B.: Development and refinement of proxy-climate indicators from peats, *Quat. Int.*, 268, 21–  
 545 33, doi:10.1016/j.quaint.2011.04.039, 2012.
- 546 Charman, D. J., Hendon, D. and Woodland, W.: The identification of testate amoebae (Protozoa: Rhizopoda) in  
 547 peats, QRA Techni., Quaternary Research Association, London., 2000.
- 548 Cremaschi, M. and Zerboni, A.: Early to Middle Holocene landscape exploitation in a drying environment: Two  
 549 case studies compared from the central Sahara (SW Fezzan, Libya), *Comptes Rendus - Geosci.*, 341(8–9), 689–  
 550 702, doi:10.1016/j.crte.2009.05.001, 2009.
- 551 Cristea, G., Cuna, S. M., Farcas, S., Tantau, I., Dordai, E. and Magdas, D. A.: Carbon isotope composition as  
 552 indicator for climatic changes during the middle and late Holocene in a peat bog from Maramures Mountains  
 553 (Romania), *The Holocene*, 24, 15–23, doi:10.1177/0959683613512166, 2013.
- 554 Cristea, V.: *Fitosociologie și vegetația României*, Babes-Bolyai University Press, Cluj Napoca., 1993.
- 555 Croudace, I. W., Rindby, A. and Rothwell, R. G.: ITRAX: description and evaluation of a new multi-function  
 556 X-ray core scanner, *Geol. Soc. London*, 267, 51–63, doi:10.1144/GSL.SP.2006.267.01.04, 2006.
- 557 Davis, B. A. S., Brewer, S., Stevenson, A. C. and Guiot, J.: The temperature of Europe during the Holocene  
 558 reconstructed from pollen data, *Quat. Sci. Rev.*, 22(15–17), 1701–1716, doi:10.1016/S0277-3791(03)00173-2,  
 559 2003.
- 560 Debret, M., Bout-Roumzeilles, V., Grousset, F., Desmet, M., McManus, J. F., Massei, N., Sebag, D., Petit, J.-  
 561 R., Copard, Y. and Trentesaux, A.: The origin of the 1500-year climate cycles in Holocene North-Atlantic  
 562 records, *Clim. Past Discuss.*, 3(2), 679–692, doi:10.5194/cpd-3-679-2007, 2007.
- 563 deMenocal, P., Ortiz, J., Guilderson, T., Adkins, J., Sarnthein, M., Baker, L. and Yarusinsky, M.: Abrupt onset  
 564 and termination of the African Humid Period: rapid climate responses to gradual insolation forcing, *Quat. Sci.*  
 565 *Rev.*, 19(1), 347–361, doi:10.1016/S0277-3791(99)00081-5, 2000.
- 566 deMenocal, P. B.: Cultural responses to climate change during the late Holocene, *Science* (80- ), 292(5517),  
 567 667–673, doi:10.1126/science.1059287, 2001.
- 568 Diaconu, A.-C., Grindean, R., Panait, A. and Tanțău, I.: Late Holocene palaeohydrological changes in a  
 569 *Sphagnum* peat bog from NW Romania based on testate amoebae, *Stud. UBB Geol.*, 60(1),  
 570 doi:http://dx.doi.org/10.5038/1937-8602.60.1.1285, 2016.
- 571 Drăgușin, V., Staubwasser, M., Hoffmann, D. L., Ersek, V., Onac, B. P. and Veres, D.: Constraining Holocene  
 572 hydrological changes in the Carpathian–Balkan region using speleothem  $\delta^{18}\text{O}$  and pollen-based temperature  
 573 reconstructions, *Clim. Past*, 10(4), 1363–1380, doi:10.5194/cp-10-1363-2014, 2014.
- 574 Edri, A., Dody, A., Tanner, S., Swet, N. and Katra, I.: Variations in dust-related PM10 emission from an arid  
 575 land due to surface composition and topsoil disturbance, *Arab. J. Geosci.*, 9(12), 607, doi:10.1007/s12517-016-  
 576 2651-z, 2016.
- 577 Egerer, S., Claussen, M., Reick, C. and Stanelle, T.: The link between marine sediment records and changes in  
 578 Holocene Saharan landscape: simulating the dust cycle, *Clim. Past*, 12(4), 1009–1027, doi:10.5194/cp-12-1009-  
 579 2016, 2016.



- 580 Feurdean, A., Klotz, S., Mosbrugger, V. and Wohlfarth, B.: Pollen-based quantitative reconstructions of  
 581 Holocene climate variability in NW Romania, *Palaeogeogr. Palaeoclimatol. Palaeoecol.*, 260(3–4), 494–504,  
 582 doi:10.1016/j.palaeo.2007.12.014, 2008.
- 583 Feurdean, A., Tămaş, T., Tanţău, I. and Fărcaş, S.: Elevational variation in regional vegetation responses to late-  
 584 glacial climate changes in the Carpathians, *J. Biogeogr.*, 39(2), 258–271, doi:10.1111/j.1365-  
 585 2699.2011.02605.x, 2012.
- 586 Feurdean, A., Galka, M., Kuske, E., Tantau, I., Lamentowicz, M., Florescu, G., Liakka, J., Hutchinson, S. M.,  
 587 Mulch, A. and Hickler, T.: Last Millennium hydro-climate variability in Central-Eastern Europe (Northern  
 588 Carpathians, Romania), *The Holocene*, 25(7), 1179–1192, doi:10.1177/0959683615580197, 2015.
- 589 Fletcher, W. J., Debret, M. and Goni, M. F. S.: Mid-Holocene emergence of a low-frequency millennial  
 590 oscillation in western Mediterranean climate: Implications for past dynamics of the North Atlantic atmospheric  
 591 westerlies, *The Holocene*, 23(2), 153–166, doi:10.1177/0959683612460783, 2013.
- 592 Francus, P., Lamb, H., Nakagawa, T., Marshall, M., Brown, E. and Members, S. 2006 P.: The potential of high-  
 593 resolution X-ray fluorescence core scanning : Applications in paleolimnology, *PAGES news*, 17(3), 93–95,  
 594 2009.
- 595 Galka, M., Tanţău, I., Ersek, V. and Feurdean, A.: A 9000year record of cyclic vegetation changes identified in  
 596 a montane peatland deposit located in the Eastern Carpathians (Central-Eastern Europe): Autogenic succession  
 597 or regional climatic influences?, *Palaeogeogr. Palaeoclimatol. Palaeoecol.*, 449, 52–61,  
 598 doi:10.1016/j.palaeo.2016.02.007, 2016.
- 599 Giosan, L., Coolen, M. J. L., Kaplan, J. O., Constantinescu, S., Filip, F., Filipova-Marinova, M., Kettner, A. J.  
 600 and Thom, N.: Early Anthropogenic Transformation of the Danube-Black Sea System, *Sci. Rep.*, 2, 1–6,  
 601 doi:10.1038/srep00582, 2012.
- 602 Goudie, A. S. and Middleton, N. J.: *Desert Dust in the Global System*, Springer Berlin Heidelberg, Berlin  
 603 Heidelberg, 2006.
- 604 Grinsted, A., Moore, J. C. and Jevrejeva, S.: Application of the cross wavelet transform and wavelet coherence  
 605 to geophysical time series, *Nonlinear Process. Geophys.*, 11(5/6), 561–566, 2004.
- 606 Grousset, F. E. and Biscaye, P. E.: Tracing dust sources and transport patterns using Sr, Nd and Pb isotopes,  
 607 *Chem. Geol.*, 222(3), 149–167, doi:10.1016/j.chemgeo.2005.05.006, 2005.
- 608 Grousset, F. E., Ginoux, P., Bory, A. and Biscaye, P. E.: Case study of a Chinese dust plume reaching the  
 609 French Alps, *Geophys. Res. Lett.*, 30(6), 1277, doi:10.1029/2002GL016833, 2003.
- 610 Harangi, S., Molnar, M., Vinkler, A. P., Kiss, B., Jull, A. J. T. and Leonard, A. G.: Radiocarbon Dating of the  
 611 Last Volcanic Eruptions of Ciomadul Volcano, Southeast Carpathians, Eastern-Central Europe, *Radiocarbon*,  
 612 52(3), 1498–1507, 2010.
- 613 Heiri, O., Lotter, A. F. and Lemcke, G.: Loss on ignition as a method for estimating organic and carbonate  
 614 content in sediments: Reproducibility and comparability of results, *J. Paleolimnol.*, 25, 101–110,  
 615 doi:10.1023/A:1008119611481, 2001.
- 616 Jickells, T. D.: Global Iron Connections Between Desert Dust, Ocean Biogeochemistry, and Climate, *Science*  
 617 (80-. ), 308(5718), 67–71, doi:10.1126/science.1105959, 2005.
- 618 Jiménez-Espejo, F. J., García-Alix, A., Jiménez-Moreno, G., Rodrigo-Gámiz, M., Anderson, R. S., Rodríguez-  
 619 Tovar, F. J., Martínez-Ruiz, F., Giral, S., Delgado Huertas, A. and Pardo-Igúzquiza, E.: Saharan aeolian input  
 620 and effective humidity variations over western Europe during the Holocene from a high altitude record, *Chem.*  
 621 *Geol.*, 374, 1–12, doi:10.1016/j.chemgeo.2014.03.001, 2014.
- 622 Kaplan, J. O., Krumhardt, K. M. and Zimmermann, N.: The prehistoric and preindustrial deforestation of  
 623 Europe, *Quat. Sci. Rev.*, 28(27), 3016–3034, doi:10.1016/j.quascirev.2009.09.028, 2009.





- 624 Karátson, D., Wulf, S., Veres, D., Magyari, E. K., Gertisser, R., Timar-Gabor, A., Novothny, Telbisz, T., Szalai,  
 625 Z., Anechitei-Deacu, V., Appelt, O., Bormann, M., Jánosi, C., Hubay, K. and Schäbitz, F.: The latest explosive  
 626 eruptions of Ciomadul (Csomád) volcano, East Carpathians - A tephrostratigraphic approach for the 51-29 ka  
 627 BP time interval, *J. Volcanol. Geotherm. Res.*, 319, 29–51, doi:10.1016/j.jvolgeores.2016.03.005, 2016.
- 628 Kok, J. F., Mahowald, N. M., Fratini, G., Gillies, J. A., Ishizuka, M., Leys, J. F. and Mikami, M.: An improved  
 629 dust emission model – Part 1: Model description and comparison against measurements, *Atmos. Chem. Phys.*,  
 630 14, 13023–13041, doi:10.5194/acp-14-13023-2014, 2014.
- 631 Korcz, M., Fudala, J. and Kliś, C.: Estimation of wind blown dust emissions in Europe and its vicinity, *Atmos.*  
 632 *Environ.*, 43(7), 1410–1420, doi:10.1016/j.atmosenv.2008.05.027, 2009.
- 633 Korponai, J., Magyari, E. K., Buczkó, K., Iepure, S., Namiotko, T., Czakó, D., Kövér, C. and Braun, M.:  
 634 Cladocera response to Late Glacial to Early Holocene climate change in a South Carpathian mountain lake,  
 635 *Hydrobiologia*, 676(1), 223–235, doi:10.1007/s10750-011-0881-3, 2011.
- 636 Krachler, M., Mohl, C., Emons, H. and Shoty, W.: Influence of digestion procedures on the determination of  
 637 rare earth elements in peat and plant samples by USN-ICP-MS, *J. Anal. At. Spectrom.*, 17(8), 844–851,  
 638 doi:10.1039/b200780k, 2002.
- 639 Kristó, A.: A Csomád hegycsoport. A Szent-Anna tó természetvédelmi területe (The Nature Reserve of Lake  
 640 Saint Ana), Kristó András emlékére (In Rememb. András Kristó). Balat. Akadémia Könyvek, 13, 38–45, 1995.
- 641 Kylander, M. E., Ampel, L., Wohlfarth, B. and Veres, D.: High-resolution X-ray fluorescence core scanning  
 642 analysis of Les Echets (France) sedimentary sequence: new insights from chemical proxies, *J. Quat. Sci.*, 26(1),  
 643 109–117, doi:10.1002/jqs.1438, 2011.
- 644 Kylander, M. E., Bindler, R., Cortizas, A. M., Gallagher, K., Mörth, C. M. and Rauch, S.: A novel geochemical  
 645 approach to paleorecords of dust deposition and effective humidity: 8500 years of peat accumulation at Store  
 646 Mosse (the “Great Bog”), Sweden, *Quat. Sci. Rev.*, 69, 69–82, doi:10.1016/j.quascirev.2013.02.010, 2013.
- 647 Labzovskii, L., Toanca, F. and Nicolae, D.: Determination of Saharan dust properties over Bucharest, Romania.  
 648 Part 2: Study cases analysis, *Rom. J. Phys.*, 59(9–10), 1097–1108, 2014.
- 649 Lamentowicz, M., Cedro, A., Galka, M., Goslar, T., Miotk-Szpiganowicz, G., Mitchell, E. A. D. and Pawlyta,  
 650 J.: Last millennium palaeoenvironmental changes from a Baltic bog (Poland) inferred from stable isotopes,  
 651 pollen, plant macrofossils and testate amoebae, *Palaeogeogr. Palaeoclimatol. Palaeoecol.*, 265(1), 93–106,  
 652 doi:10.1016/j.palaeo.2008.04.023, 2008.
- 653 Longman, J., Ersek, V., Veres, D. and Salzmann, U.: Detrital events and hydroclimate variability in the  
 654 Romanian Carpathians during the Mid-to-Late Holocene, *Quat. Sci. Rev.*, n.d.
- 655 Lüdecke, H.-J., Weiss, C. O. and Hempelmann, A.: Paleoclimate forcing by the solar De Vries/Suess cycle,  
 656 *Clim. Past Discuss.*, 11(1), 279–305, doi:10.5194/cpd-11-279-2015, 2015.
- 657 Magny, M.: Holocene climate variability as reflected by mid-European lake-level fluctuations and its probable  
 658 impact on prehistoric human settlements, *Quat. Int.*, 113(1), 65–79, doi:10.1016/S1040-6182(03)00080-6, 2004.
- 659 Magny, M., Combourieu-Nebout, N., De Beaulieu, J. L., Bout-Roumazeilles, V., Colombaroli, D., Desprat, S.,  
 660 Francke, A., Joannin, S., Ortu, E. and Peyron, O.: Geoscientific Instrumentation Methods and Data Systems  
 661 North–south palaeohydrological contrasts in the central Mediterranean during the Holocene: tentative synthesis  
 662 and working hypotheses, *Clim. Past*, 9, 2043–2071, doi:10.5194/cp-9-2043-2013, 2013.
- 663 Magyari, E., Buczkó, K., Jakab, G., Braun, M., Pál, Z., Karátson, D. and Pap, I.: Palaeolimnology of the last  
 664 crater lake in the Eastern Carpathian Mountains: a multiproxy study of Holocene hydrological changes., 2009.
- 665 Magyari, E. K., Chapman, J. C., Passmore, D. G., Allen, J. R. M., Huntley, J. P. and Huntley, B.: Holocene  
 666 persistence of wooded steppe in the Great Hungarian Plain, *J. Biogeogr.*, 37, 915–935, doi:10.1111/j.1365-  
 667 2699.2009.02261.x, 2010.



- 668 Magyari, E. K., Jakab, G., Bálint, M., Kern, Z., Buczkó, K. and Braun, M.: Rapid vegetation response to  
 669 Lateglacial and early Holocene climatic fluctuation in the South Carpathian Mountains (Romania), *Quat. Sci.*  
 670 *Rev.*, 35, 116–130, doi:10.1016/j.quascirev.2012.01.006, 2012.
- 671 Magyari, E. K., Demény, A., Buczkó, K., Kern, Z., Vennemann, T., Fórizs, I., Vincze, I., Braun, M., Kovács, J.  
 672 I., Udvardi, B. and Veres, D.: A 13,600-year diatom oxygen isotope record from the South Carpathians  
 673 (Romania): Reflection of winter conditions and possible links with North Atlantic circulation changes, *Quat.*  
 674 *Int.*, 293, 136–149, doi:10.1016/j.quaint.2012.05.042, 2013.
- 675 Magyari, E. K., Veres, D., Wennrich, V., Wagner, B., Braun, M., Jakab, G., Karátson, D., Pál, Z., Ferenczy, G.,  
 676 St-Onge, G., Rethemeyer, J., Francois, J.-P., von Reumont, F. and Schäbitz, F.: Vegetation and environmental  
 677 responses to climate forcing during the Last Glacial Maximum and deglaciation in the East Carpathians:  
 678 attenuated response to maximum cooling and increased biomass burning, *Quat. Sci. Rev.*, 106, 278–298,  
 679 doi:10.1016/j.quascirev.2014.09.015, 2014.
- 680 Mahowald, N. M., Kloster, S., Engelstaedter, S., Moore, J. K., Mukhopadhyay, S., McConnell, J. R., Albani, S.,  
 681 Doney, S. C., Bhattacharya, A., Curran, M. A. J., Flanner, M. G., Hoffman, F. M., Lawrence, D. M., Lindsay,  
 682 K., Mayewski, P. A., Neff, J., Rothenberg, D., Thomas, E., Thornton, P. E. and Zender, C. S.: Observed 20th  
 683 century desert dust variability: impact on climate and biogeochemistry, *Atmos. Chem. Phys. Atmos. Chem.*  
 684 *Phys.*, 10, 10875–10893, doi:10.5194/acp-10-10875-2010, 2010.
- 685 Mann, M. E., Zhang, Z., Rutherford, S., Bradley, R. S., Hughes, M. K., Shindell, D., Ammann, C., Faluvegi, G.  
 686 and Ni, F.: Global Signatures and Dynamical Origins of the Little Ice Age and Medieval Climate Anomaly,  
 687 *Science* (80-. ), 326(5957), 1256–1260, doi:10.1126/science.1177303, 2009.
- 688 Marković, S. B., Stevens, T., Kukla, G. J., Hambach, U., Fitzsimmons, K. E., Gibbard, P., Buggle, B., Zech, M.,  
 689 Guo, Z., Hao, Q., Wu, H., O'Hara Dhand, K., Smalley, I. J., Újvári, G., Sümegi, P., Timar-Gabor, A., Veres, D.,  
 690 Sirocko, F., Vasiljević, D. A., Jary, Z., Svensson, A., Jović, V., Lehmkuhl, F., Kovács, J. and Svirčev, Z.:  
 691 Danube loess stratigraphy — Towards a pan-European loess stratigraphic model, *Earth-Science Rev.*, 148, 228–  
 692 258, doi:10.1016/j.earscirev.2015.06.005, 2015.
- 693 Marx, S. K., McGowan, H. A. and Kamber, B. S.: Long-range dust transport from eastern Australia: A proxy for  
 694 Holocene aridity and ENSO-type climate variability., 2009.
- 695 Marx, S. K., Kamber, B. S., McGowan, H. a. and Zawadzki, A.: Atmospheric pollutants in alpine peat bogs  
 696 record a detailed chronology of industrial and agricultural development on the Australian continent, *Environ.*  
 697 *Pollut.*, 158(5), 1615–1628, doi:10.1016/j.envpol.2009.12.009, 2010.
- 698 Mauri, A., Davis, B. A. S., Collins, P. M. and Kaplan, J. O.: The climate of Europe during the Holocene: a  
 699 gridded pollen-based reconstruction and its multi-proxy evaluation, *Quat. Sci. Rev.*, 112, 109–127,  
 700 doi:10.1016/j.quascirev.2015.01.013, 2015.
- 701 Mayewski, P. a, Rohling, E., Curtstager, J., Karlén, W., Maasch, K., Davidmeeker, L., Meyerson, E., Gasse, F.,  
 702 Vankreveld, S. and Holmgren, K.: Holocene climate variability, *Quat. Res.*, 62(3), 243–255,  
 703 doi:10.1016/j.yqres.2004.07.001, 2004.
- 704 McGee, D., deMenocal, P. B., Winckler, G., Stuut, J. B. W. and Bradtmiller, L. I.: The magnitude, timing and  
 705 abruptness of changes in North African dust deposition over the last 20,000yr., 2013.
- 706 Miao, X., Mason, J. A., Swinehart, J. B., Loope, D. B., Hanson, P. R., Goble, R. J. and Liu, X.: A 10,000 year  
 707 record of dune activity, dust storms, and severe drought in the central Great Plains, *Geology*, 35(2), 119,  
 708 doi:10.1130/G23133A.1, 2007.
- 709 Molnár, M., Rinyu, L., Veres, M., Seiler, M., Wacker, L. and Synal, H.-A.: EnvironMICADAS : a mini 14C  
 710 AMS with enhanced gas ion source, *Radiocarbon*, 55(2), 338–344, doi:10.2458/azu\_js\_rc.55.16331, 2013.
- 711 Morellón, M., Anselmetti, F. S., Ariztegui, D., Brushulli, B., Sinopoli, G., Wagner, B., Sadori, L., Gilli, A. and  
 712 Pambuku, A.: Human–climate interactions in the central Mediterranean region during the last millennia: The  
 713 laminated record of Lake Butrint (Albania), *Quat. Sci. Rev.*, 136, 134–152,  
 714 doi:10.1016/j.quascirev.2015.10.043, 2016.



- 715 Moreno, T., Querol, X., Castillo, S., Alastuey, A., Cuevas, E., Herrmann, L., Mounkaila, M., Elvira, J. and  
 716 Gibbons, W.: Geochemical variations in aeolian mineral particles from the Sahara–Sahel Dust Corridor,  
 717 *Chemosphere*, 65(2), 261–270, doi:10.1016/j.chemosphere.2006.02.052, 2006.
- 718 Morley, A., Rosenthal, Y. and deMenocal, P.: Ocean-atmosphere climate shift during the mid-to-late Holocene  
 719 transition., 2014.
- 720 Morris, P. J., Baird, A. J., Young, D. M. and Swindles, G. T.: Untangling climate signals from autogenic  
 721 changes in long-term peatland development, *Geophys. Res. Lett.*, 42(24), 10,788–10,797,  
 722 doi:10.1002/2015GL066824, 2015.
- 723 Mulitza, S., Heslop, D., Pittauerova, D., Fischer, H. W., Meyer, I., Stuut, J.-B., Zabel, M., Mollenhauer, G.,  
 724 Collins, J. A., Kuhnert, H. and Schulz, M.: Increase in African dust flux at the onset of commercial agriculture  
 725 in the Sahel region, *Nature*, 466(7303), 226–228, doi:10.1038/nature09213, 2010.
- 726 Nichols, J. E. and Huang, Y.: Hydroclimate of the northeastern United States is highly sensitive to solar forcing,  
 727 *Geophys. Res. Lett.*, 39(4), n/a-n/a, doi:10.1029/2011GL050720, 2012.
- 728 Nicolás, J., Chiari, M., Crespo, J., Orellana, I. G., Lucarelli, F., Nava, S., Pastor, C. and Yubero, E.:  
 729 Quantification of Saharan and local dust impact in an arid Mediterranean area by the positive matrix  
 730 factorization (PMF) technique, *Atmos. Environ.*, 42(39), 8872–8882, doi:10.1016/j.atmosenv.2008.09.018,  
 731 2008.
- 732 Notaro, M., Yu, Y. and Kalashnikova, O. V.: Regime shift in Arabian dust activity, triggered by persistent  
 733 Fertile Crescent drought, *J. Geophys. Res. Atmos.*, 120(19), 10,229–10,249, doi:10.1002/2015JD023855, 2015.
- 734 Novak, M., Zemanova, L., Voldrichova, P., Stepanova, M., Adamova, M., Pachero, P., Komarek, A.,  
 735 Krachler, M. and Prechova, E.: Experimental Evidence for Mobility/Immobility of Metals in Peat, *Environ. Sci.*  
 736 *Technol.*, 45(17), 7180–7187, doi:10.1021/es201086v, 2011.
- 737 Obrecht, I., Zeeden, C., Hambach, U., Veres, D., Marković, S. B., Bösken, J., Svirčev, Z., Bačević, N., Gavrilov,  
 738 M. B. and Lehmkuhl, F.: Tracing the influence of Mediterranean climate on Southeastern Europe during the past  
 739 350,000 years, *Sci. Rep.*, 6, 36334, doi:10.1038/srep36334, 2016.
- 740 Poore, R. Z., Quinn, T. M. and Verardo, S.: Century-scale movement of the Atlantic Intertropical Convergence  
 741 Zone linked to solar variability, *Geophys. Res. Lett.*, 31(12), n/a-n/a, doi:10.1029/2004GL019940, 2004.
- 742 Pop, E.: Mlaștinile de turbă din Republica Populară Română (Peat bogs from Romania), Editura Academiei  
 743 Republicii Populare Române, Bucharest., 1960.
- 744 Poto, L., Gabrieli, J., Crowhurst, S., Agostinelli, C., Spolaor, A., Cairns, W. R. L., Cozzi, G. and Barbante, C.:  
 745 Cross calibration between XRF and ICP-MS for high spatial resolution analysis of ombrotrophic peat cores for  
 746 palaeoclimatic studies, *Anal. Bioanal. Chem.*, 407, 379–385, doi:10.1007/s00216-014-8289-3, 2014.
- 747 Ramanathan, V.: Aerosols, Climate, and the Hydrological Cycle, *Science* (80-. ), 294(5549), 2119–2124,  
 748 doi:10.1126/science.1064034, 2001.
- 749 Rasmussen, S. O., Vinther, B. M., Clausen, H. B. and Andersen, K. K.: Early Holocene climate oscillations  
 750 recorded in three Greenland ice cores, *Quat. Sci. Rev.*, 26(15–16), 1907–1914,  
 751 doi:10.1016/j.quascirev.2007.06.015, 2007.
- 752 Reimer, P., Bard, E., Bayliss, A., Beck, J. W., Blackwell, P. G., Bronk Ramsey, C., Buck, C. E., Cheng, H.,  
 753 Edwards, R. L., Friedrich, M., Grootes, P. M., Guilderson, T. P., Hafliðason, H., Hajdas, I., Hatté, C., Heaton, T.,  
 754 J., Hoffmann, D. L., Hogg, A. G., Hughen, K. A., Kaiser, K. F., Kromer, B., Manning, S. W., Niu, M., Reimer,  
 755 R. W., Richards, D. A., Scott, E. M., Southon, J. R., Staff, R. A., Turney, C. S. M. and van der Plicht, J.:  
 756 IntCal13 and Marine13 Radiocarbon Age Calibration Curves 0–50,000 Years cal BP, *Radiocarbon*, 55(4),  
 757 1869–1887, doi:10.2458/azu\_js\_rc.55.16947, 2013.
- 758 Revel, M., Ducassou, E., Grousset, F. E., Bernasconi, S. M., Migeon, S., Revillon, S., Mascle, J., Murat, A.,  
 759 Zaragosi, S. and Bosch, D.: 100,000 Years of African monsoon variability recorded in sediments of the Nile



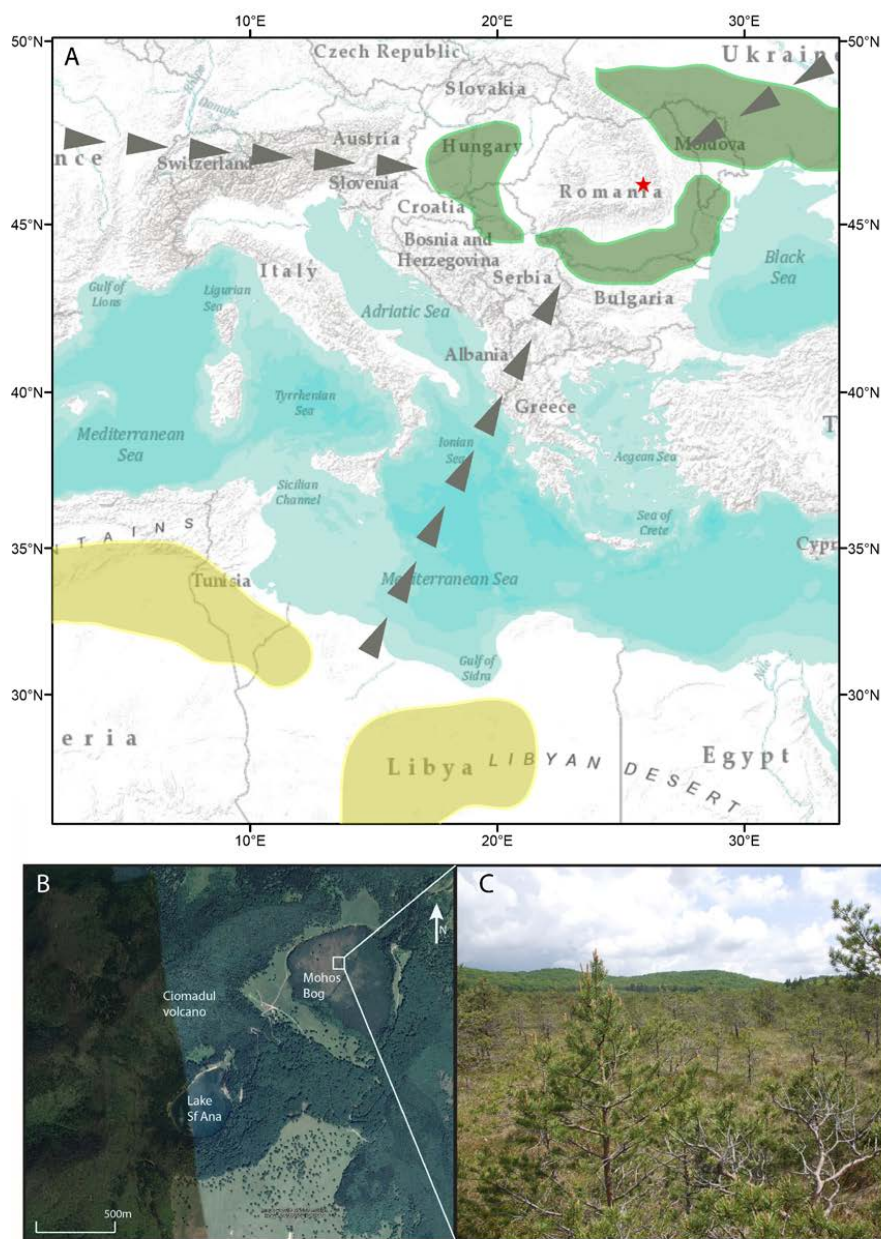
- 760 margin, *Quat. Sci. Rev.*, 29(11), 1342–1362, doi:10.1016/j.quascirev.2010.02.006, 2010.
- 761 Roberts, N., Moreno, A., Valero-Garcés, B. L., Corella, J. P., Jones, M., Allcock, S., Woodbridge, J., Morellón,  
762 M., Luterbacher, J., Xoplaki, E. and Türkeş, M.: Palaeolimnological evidence for an east-west climate see-saw  
763 in the Mediterranean since AD 900, *Glob. Planet. Change*, 84–85, 23–34, doi:10.1016/j.gloplacha.2011.11.002,  
764 2012.
- 765 Ross-Barracough, F. and Shotyk, W.: Millennial-scale records of atmospheric mercury deposition obtained  
766 from ombrotrophic and minerotrophic peatlands in the Swiss Jura Mountains, *Environ. Sci. Technol.*, 37(2),  
767 235–244, doi:10.1021/es0201496, 2003.
- 768 Rothwell, J. J., Taylor, K. G., Chenery, S. R. N., Cundy, A. B., Evans, M. G. and Allott, T. E. H.: Storage and  
769 behavior of As, Sb, Pb, and Cu in ombrotrophic peat bogs under contrasting water table conditions, *Environ.*  
770 *Sci. Technol.*, 44(22), 8497–8502, doi:10.1021/es101150w, 2010.
- 771 Rousseau, D.-D., Chauvel, C., Sima, A., Hatté, C., Lagroix, F., Antoine, P., Balkanski, Y., Fuchs, M., Mellett,  
772 C., Kageyama, M., Ramstein, G. and Lang, A.: European glacial dust deposits: Geochemical constraints on  
773 atmospheric dust cycle modeling, *Geophys. Res. Lett.*, 41(21), 7666–7674, doi:10.1002/2014GL061382, 2014.
- 774 Le Roux, G., Fagel, N., De Vleeschouwer, F., Krachler, M., Debaille, V., Stille, P., Mattielli, N., van der Knaap,  
775 W. O., van Leeuwen, J. F. N. and Shotyk, W.: Volcano- and climate-driven changes in atmospheric dust sources  
776 and fluxes since the Late Glacial in Central Europe, *Geology*, 40(4), 335–338, doi:10.1130/g32586.1, 2012.
- 777 Russell, J. M., Johnson, T. C. and Talbot, M. R.: A 725 yr cycle in the climate of central Africa during the late  
778 Holocene, *Geology*, 31(8), 2003.
- 779 Scheuven, D., Schütz, L., Kandler, K., Ebert, M. and Weinbruch, S.: Bulk composition of northern African dust  
780 and its source sediments — A compilation, *Earth-Science Rev.*, 116, 170–194,  
781 doi:10.1016/j.earscirev.2012.08.005, 2013.
- 782 Schnitchen, C., Charman, D. J., Magyari, E., Braun, M., Grigorszky, I., Tóthmérész, B., Molnár, M. and Szántó,  
783 Z.: Reconstructing hydrological variability from testate amoebae analysis in Carpathian peatlands, *J.*  
784 *Paleolimnol.*, 36(1), 1–17, doi:10.1007/s10933-006-0001-y, 2006.
- 785 Schumacher, M., Schier, W. and Schütt, B.: Mid-Holocene vegetation development and herding-related  
786 interferences in the Carpathian region, *Quat. Int.*, 415, 253–267, doi:10.1016/j.quaint.2015.09.074, 2016.
- 787 Shanahan, T. M., McKay, N. P., Hughen, K. A., Overpeck, J. T., Otto-Bliesner, B., Heil, C. W., King, J.,  
788 Scholz, C. A. and Peck, J.: The time-transgressive termination of the African Humid Period, *Nat. Geosci.*, 8(2),  
789 140–144, doi:10.1038/ngeo2329, 2015.
- 790 Sharifi, A., Pourmand, A., Canuel, E. A., Ferer-Tyler, E., Peterson, L. C., Aichner, B., Feakins, S. J., Daryaei,  
791 T., Djamali, M., Beni, A. N., Lahijani, H. A. K. and Swart, P. K.: Abrupt climate variability since the last  
792 deglaciation based on a high-resolution, multi-proxy peat record from NW Iran: The hand that rocked the Cradle  
793 of Civilization?, *Quat. Sci. Rev.*, 123, 215–230, doi:10.1016/j.quascirev.2015.07.006, 2015.
- 794 Shotyk, W.: The chronology of anthropogenic, atmospheric Pb deposition recorded by peat cores in three  
795 minerogenic peat deposits from Switzerland, *Sci. Total Environ.*, 292, 19–31, doi:10.1016/S0048-  
796 9697(02)00030-X, 2002.
- 797 Smalley, I., Marković, S. B. and Svirčev, Z.: Loess is [almost totally formed by] the accumulation of dust, *Quat.*  
798 *Int.*, 240(1–2), 4–11, doi:10.1016/j.quaint.2010.07.011, 2011.
- 799 Springer, G. S., Rowe, H. D., Hardt, B., Edwards, R. L. and Cheng, H.: Solar forcing of Holocene droughts in a  
800 stalagmite record from West Virginia in east-central North America, *Geophys. Res. Lett.*, 35(17), L17703,  
801 doi:10.1029/2008GL034971, 2008.
- 802 Sweeney, M. R. and Mason, J. A.: Mechanisms of dust emission from Pleistocene loess deposits, Nebraska,  
803 USA, *J. Geophys. Res. Earth Surf.*, 118(3), 1460–1471, doi:10.1002/jgrf.20101, 2013.



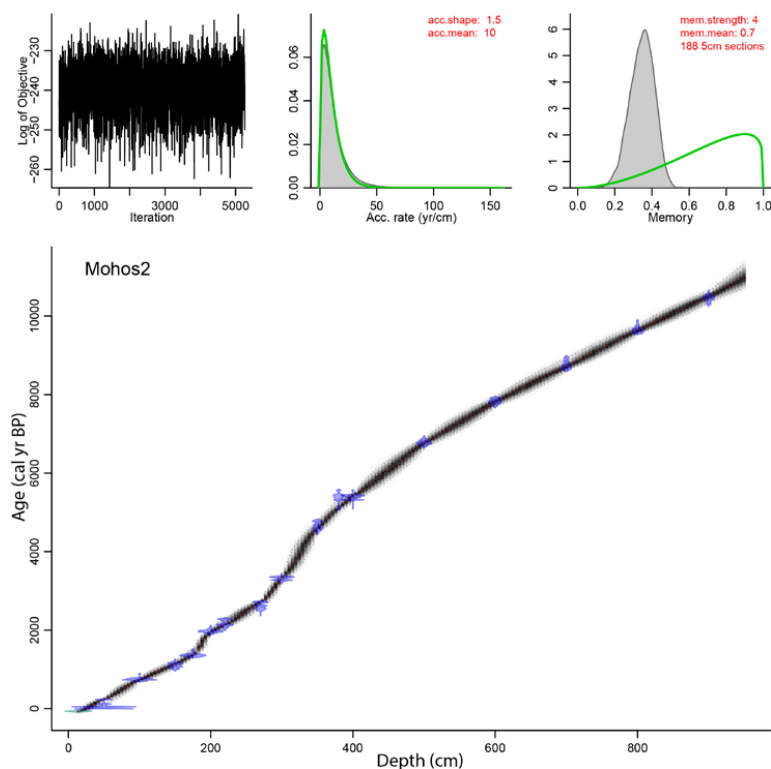
- 804 Swindles, G. T., Blundell, A., Roe, H. M. and Hall, V. A.: A 4500-year proxy climate record from peatlands in  
805 the North of Ireland: the identification of widespread summer “drought phases”?, *Quat. Sci. Rev.*, 29(13), 1577–  
806 1589, doi:10.1016/j.quascirev.2009.01.003, 2010.
- 807 Swindles, G. T., Patterson, R. T., Roe, H. M. and Galloway, J. M.: Evaluating periodicities in peat-based  
808 climate proxy records, *Quat. Sci. Rev.*, 41, 94–103, doi:10.1016/j.quascirev.2012.03.003, 2012.
- 809 Szakács, A., Seghedi, I., Pécskay, Z. and Mirea, V.: Eruptive history of a low-frequency and low-output rate  
810 Pleistocene volcano, Ciomadul, South Harghita Mts., Romania, *Bull. Volcanol.*, 77(2), 12, doi:10.1007/s00445-  
811 014-0894-7, 2015.
- 812 Tanțău, I., Reille, M., De Beaulieu, J. L., Farcas, S., Goslar, T. and Paterne, M.: Vegetation history in the  
813 Eastern Romanian Carpathians: Pollen analysis of two sequences from the Mohos crater, *Veg. Hist.*  
814 *Archaeobot.*, 12(2), 113–125, doi:10.1007/s00334-003-0015-6, 2003.
- 815 Tanțău, I., Feurdean, A., De Beaulieu, J. L., Reille, M. and Fărcaș, S.: Vegetation sensitivity to climate changes  
816 and human impact in the Harghita Mountains (Eastern Romanian Carpathians) over the past 15 000 years, *J.*  
817 *Quat. Sci.*, 29(2), 141–152, doi:10.1002/jqs.2688, 2014.
- 818 Torrence, C. and Compo, G. P.: A Practical Guide to Wavelet Analysis, *Bull. Am. Meteorol. Soc.*, 79(1), 61–78,  
819 1998.
- 820 Újvári, G., Varga, A., Ramos, F. C., Kovács, J., Németh, T. and Stevens, T.: Evaluating the use of clay  
821 mineralogy, Sr–Nd isotopes and zircon U–Pb ages in tracking dust provenance: An example from loess of the  
822 Carpathian Basin, *Chem. Geol.*, 304, 83–96, doi:10.1016/j.chemgeo.2012.02.007, 2012.
- 823 Varga, G., Kovács, J. and Újvári, G.: Analysis of Saharan dust intrusions into the Carpathian Basin (Central  
824 Europe) over the period of 1979–2011, *Glob. Planet. Change*, 100, 333–342,  
825 doi:10.1016/j.gloplacha.2012.11.007, 2013.
- 826 Varga, G., Cserhádi, C., Kovács, J. and Szalai, Z.: Saharan dust deposition in the Carpathian Basin and its  
827 possible effects on interglacial soil formation, *Aeolian Res.*, 22, 1–12, doi:10.1016/j.aeolia.2016.05.004, 2016.
- 828 Veron, A., Novak, M., Brizova, E. and Stepanova, M.: Environmental imprints of climate changes and  
829 anthropogenic activities in the Ore Mountains of Bohemia (Central Europe) since 13 cal. kyr BP, *The Holocene*,  
830 24(8), 919–931, doi:10.1177/0959683614534746, 2014.
- 831 Vinkler, A. P., Harangi, S., Ntaflos, T. and Szakács, A.: A Csornád vulkán (Keleti-Kárpátok) horzsaköveinek  
832 közzetani és geokémiai vizsgálata - petrogenetikai következtetések, , 137(1), 103–128, 2007.
- 833 Vukmirović, Z., Unkašević, M., Lazić, L., Tošić, I., Rajšić, S. and Tasić, M.: Analysis of the Saharan dust  
834 regional transport, *Meteorol. Atmos. Phys.*, 85(4), 265–273, doi:10.1007/s00703-003-0010-6, 2004.
- 835 Wanner, H., Solomina, O., Grosjean, M., Ritz, S. P. and Jetel, M.: Structure and origin of Holocene cold events,  
836 *Quat. Sci. Rev.*, 30(21–22), 3109–3123, doi:10.1016/j.quascirev.2011.07.010, 2011.
- 837 Wedepohl, K. H.: The composition of the continental crust, *Geochim. Cosmochim. Acta*, 59(7), 1217–1232,  
838 doi:10.1016/0016-7037(95)00038-2, 1995.
- 839 Wulf, S., Fedorowicz, S., Veres, D., Lanczont, M., Karátson, D., Gertisser, R., Bormann, M., Magyari, E.,  
840 Appelt, O., Hambach, U. and Gozhyk, P. F.: The “Roxolany Tephra” (Ukraine) – new evidence for an origin  
841 from Ciomadul volcano, East Carpathians, *J. Quat. Sci.*, 31(6), 565–576, doi:10.1002/jqs.2879, 2016.
- 842 Yoshioka, M., Mahowald, N. M., Conley, A. J., Collins, W. D., Fillmore, D. W., Zender, C. S. and Coleman, D.  
843 B.: Impact of desert dust radiative forcing on sahel precipitation: Relative importance of dust compared to sea  
844 surface temperature variations, vegetation changes, and greenhouse gas warming, *J. Clim.*, 20(8), 1445–1467,  
845 doi:10.1175/JCLI4056.1, 2007.
- 846 Yu, S.-Y.: Centennial-scale cycles in middle Holocene sea level along the southeastern Swedish Baltic coast,



847 Geol. Soc. Am. Bull., 115(11), 1404, doi:10.1130/B25217.1, 2003.

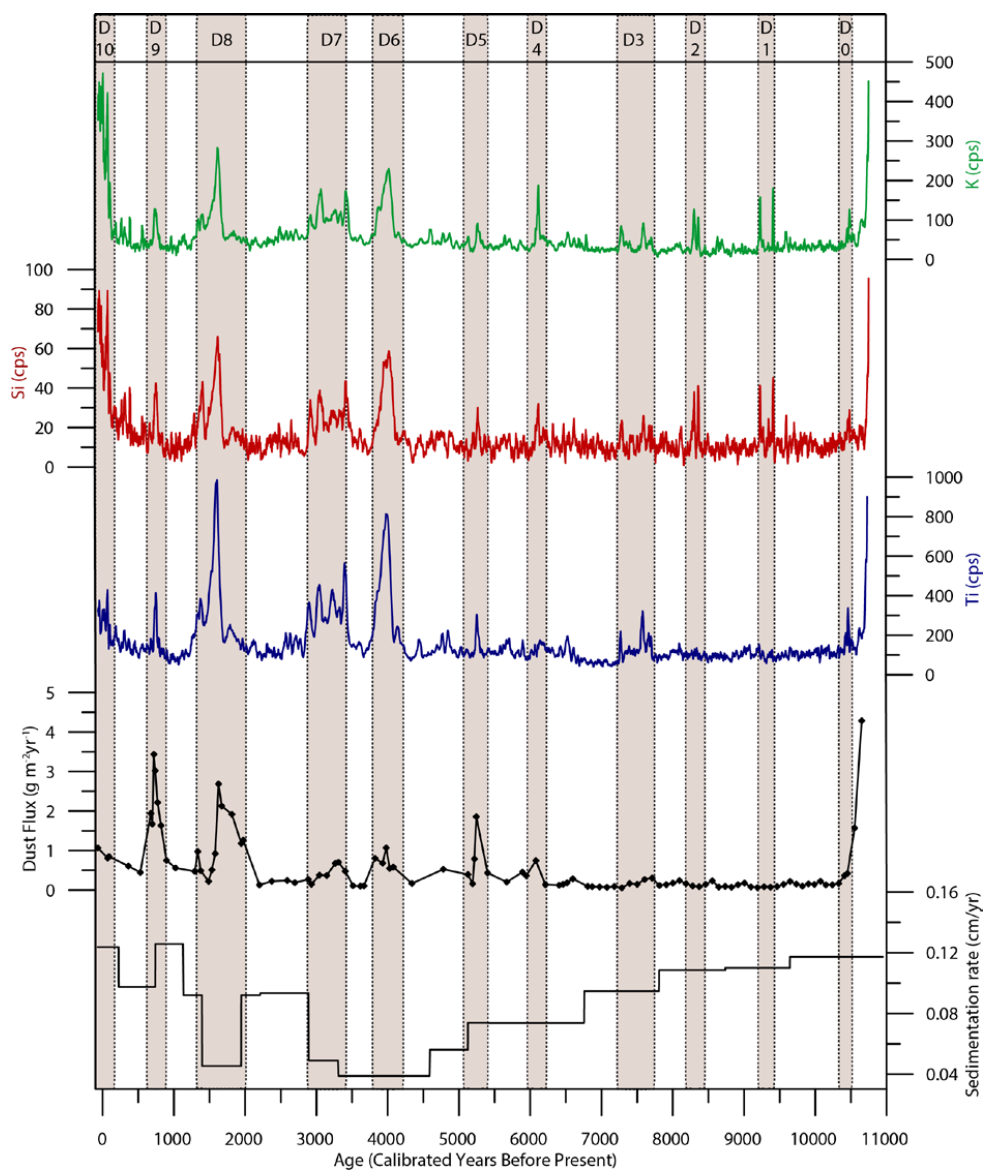


848  
849 Figure 1: 1.A: Map of the Carpathian-Balkan region indicating location of Mohos peat bog (red star),  
850 in the South-Eastern Carpathian Mountains. Predominant wind directions relating to air circulation patterns in the  
851 area are indicated by black arrows. Major Saharan dust source areas are indicated in yellow (Scheuvs et al., 2013)  
852 and local loess fields (including loess-derived alluvium) in green (Marković et al., 2015). 1.B: Map of Mohos and  
853 neighbouring Lake Sf Ana, from Google Earth 6.1.7601.1 (June 10th 2016). Harghita County, Romania, 46°05' N ;  
854 25°55' E, Eye alt 3.06 km, CNAS/Astrium, DigitalGlobe 2016. <http://www.google.com/earth/index.html> (Accessed  
855 January 23rd 2017). Coring location within white box. 1.C: Photo of Mohos bog at the coring location with the crater  
856 rim visible in the distance.



857

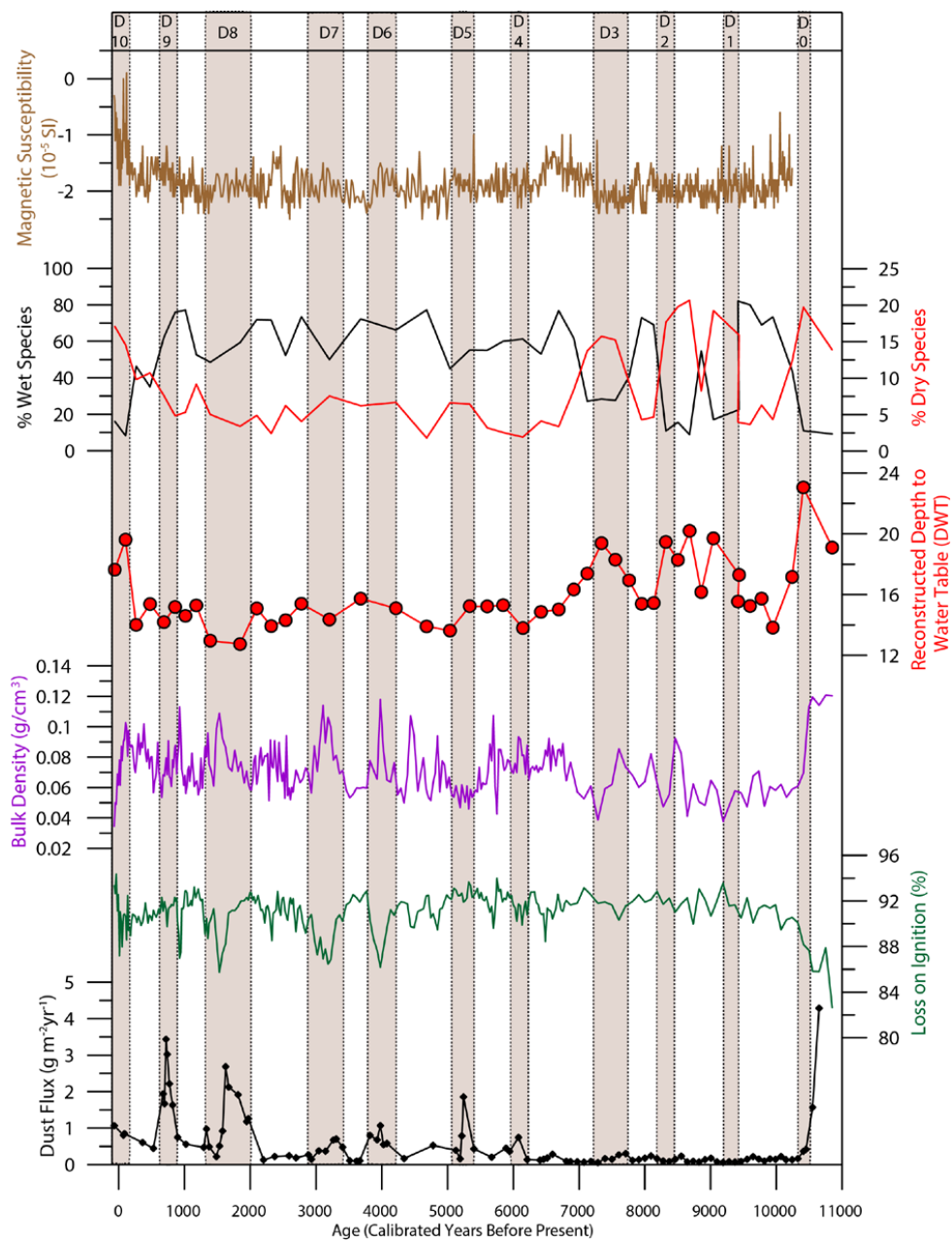
858 Figure 2: Age-depth model of Mohos peat record, as determined via Bacon (Blaauw and Christen, 2011). Upper left  
859 graph indicates Markov Chain Monte Carlo iterations. Also on the upper panel are prior (green line) and posterior  
860 (grey histogram) distributions for the accumulation rate (middle) and memory (right). For the lower panel,  
861 calibrated radiocarbon ages are in blue. The age-depth model is outlined in grey, with darker grey indicating more  
862 likely calendar ages. Grey stippled lines show 95% confidence intervals, and the red curve indicates the single 'best'  
863 model used in this work.



864  
865  
866  
867  
868

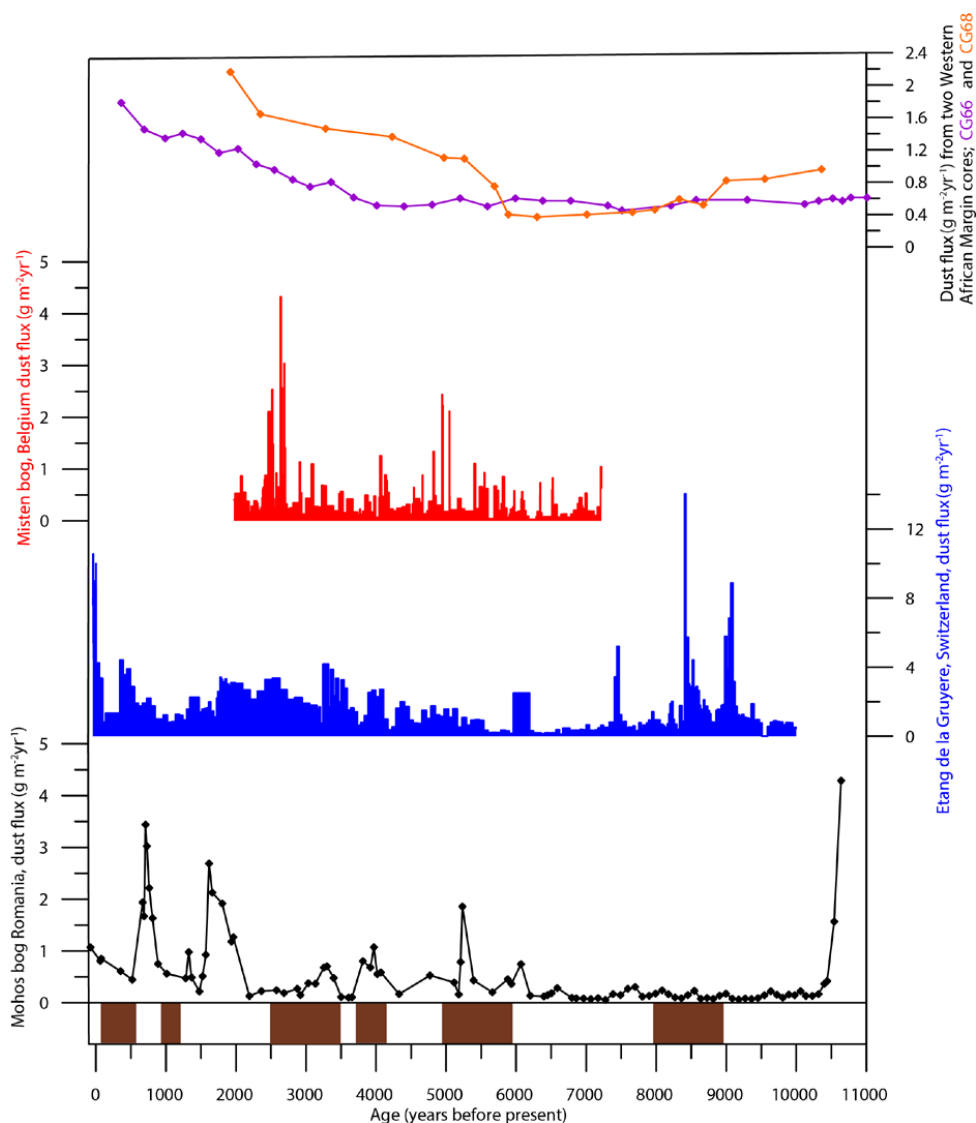
Figure 3: ITRAX data of lithogenic elements (K, Si and Ti) concentration throughout the Mohos peat record, with all data smoothed using a 10-point moving average to eliminate noise. Alongside, dust flux as reconstructed by Ti concentration values, and sedimentation rate is presented. Dust events (D0-D10), as identified from increases in at least two of the lithogenic elements under discussion, are highlighted in brown.



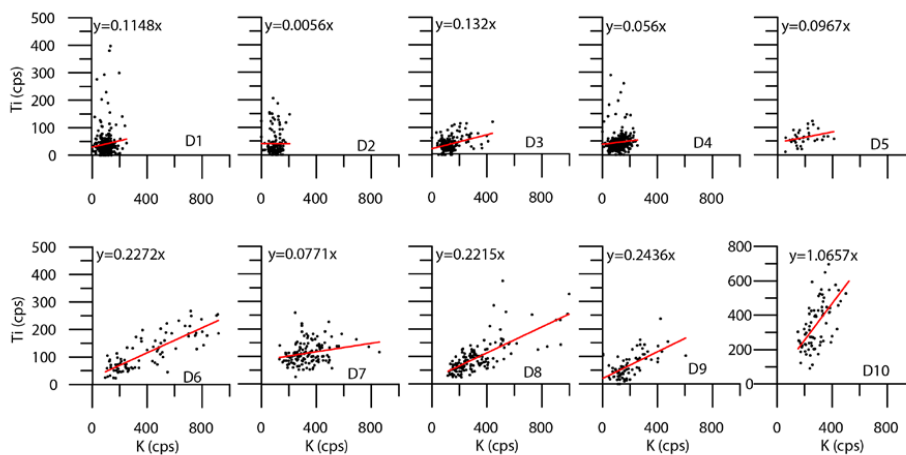


869

870 **Figure 4:** Comparison of Ti-derived dust flux record with magnetic susceptibility ( $10^{-5}$  SI), wet and dry TA indicator  
 871 species % values, reconstructed Depth to Water Table (DWT), organic matter and dry density. Vertical bars as in  
 872 Fig. 3.



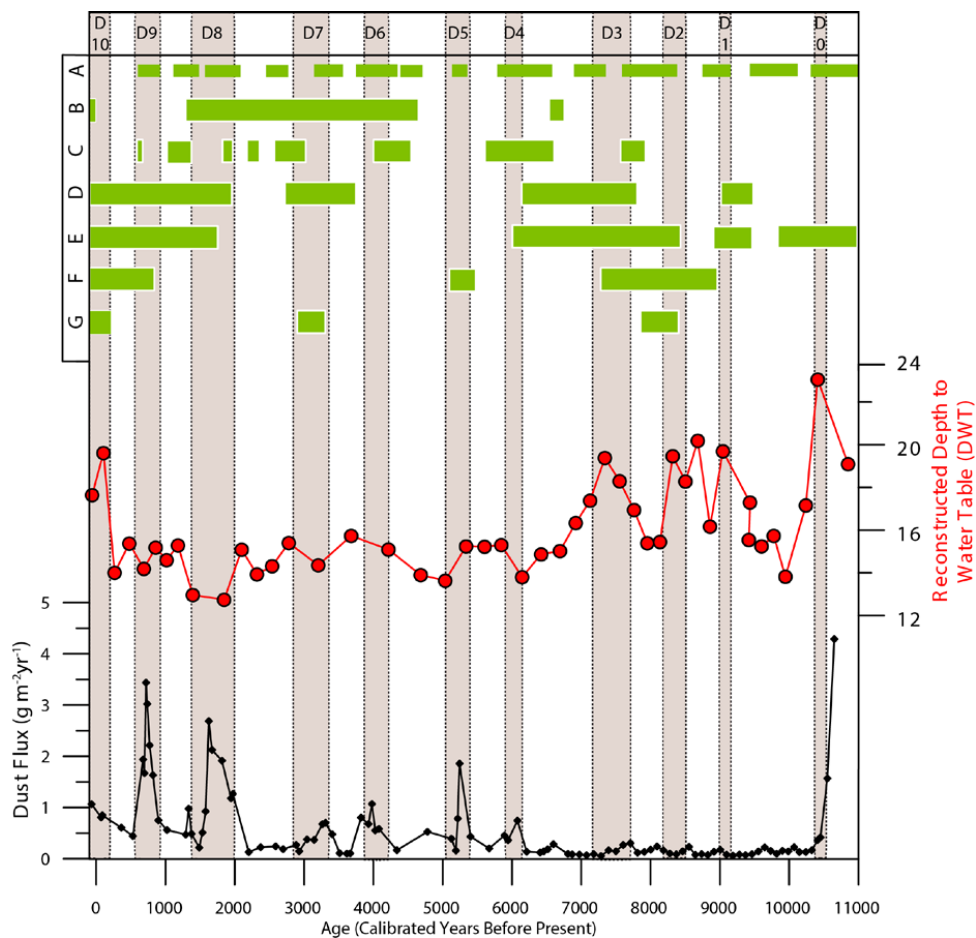
873  
874  
875 **Figure 5: Comparison of dust flux values as reconstructed from Mohos peat bog with similar records. Two Western**  
876 **African dust flux records (GC 68 and 66) from marine cores (McGee et al., 2013), are presented alongside bog-based**  
877 **records from Misten bog in Belgium (Allen et al., 2013) and Etang de la Gruyere in Switzerland (Le Roux et al., 2012)**  
878 **respectively. These are presented alongside the dust flux record from Mohos (lower panel). Also shown, in brown, are**  
879 **periods of Rapid Climate Change derived from Greenland Ice (Mayewski et al., 2004).**



880

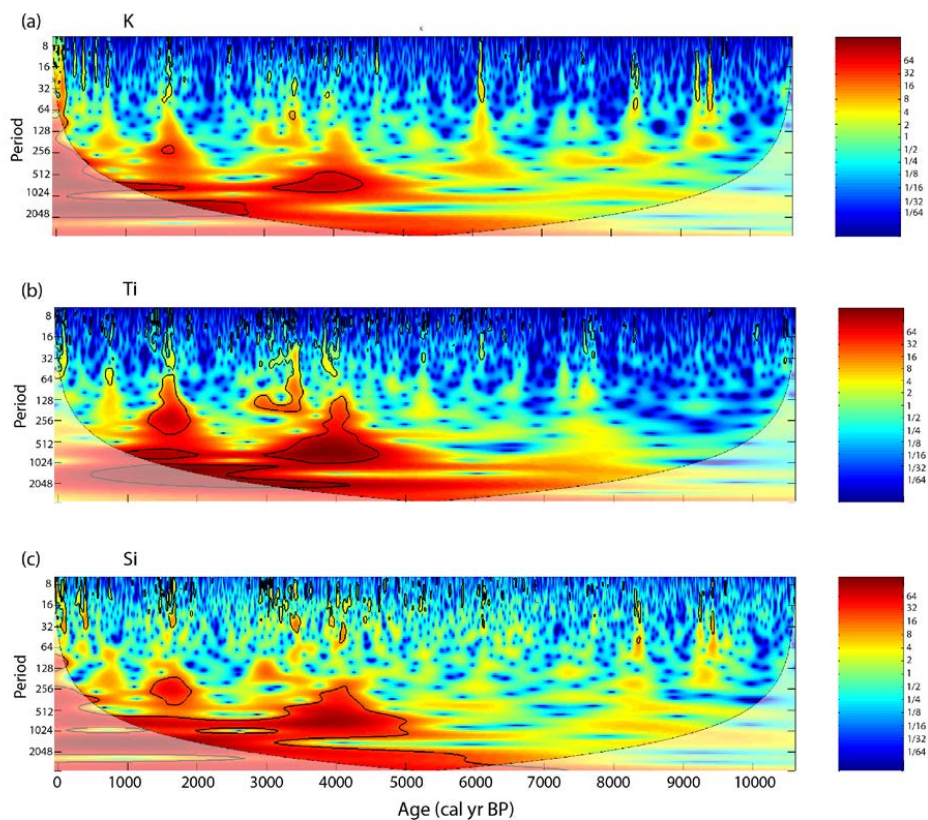
881 **Figure 6: Correlation graphs and gradients of Ti versus K for each of the dust events (D1-D10)**

882



883

884 Figure 7: Comparison of dust events and bog wetness as reconstructed from the Mohos record, to regional  
 885 hydroclimate reconstructions. Data presented via green bars is drought/dry/low lake periods from the following  
 886 publications. A: (Magny, 2004), B: (Cristea et al., 2013), C: (Galka et al., 2016), D: (Magyari et al., 2013), E: (Buczko  
 887 et al., 2013), F: (Magyari et al., 2009), G: (Schnitchen et al., 2006). These are presented alongside the Mohos Ti  
 888 record, Ti-derived dust flux.



889  
890 **Figure 8: Spectral analysis of Mohos ITRAX geochemical data for A: Ti, B: K, C: Si. Areas outlined in black are**  
891 **significant at the 95% confidence level. Shaded area indicates the cone of influence, outside of which results may be**  
892 **unreliable.**

893

894

895

896

897

898

899

900

901

902

903



904 **Table 1: Radiocarbon dates used to build the age model for Mohos peat record.**

Lab ID	Depth	<sup>14</sup> C age (yr BP ± 1σ)	Calibrated age (cal yr BP ± 2σ)	Dated material
DeA-8343	50	<b>37±18</b>	37-65	bulk peat
DeA-8344	100	<b>838±19</b>	700-785	bulk peat
DeA-10111	150	<b>1174±28</b>	1049-1179	bulk peat
DeA-10112	175	<b>1471±26</b>	1309-1399	bulk peat
DeA-8345	200	<b>2022±21</b>	1921-2007	bulk peat
DeA-10137	225	<b>2155±27</b>	2048-2305	bulk peat
DeA-10138	280	<b>2530±28</b>	2495-2744	bulk peat
DeA-8346	300	<b>3112±23</b>	3249-3383	bulk peat
DeA-10139	350	<b>4110±31</b>	4523-4713	bulk peat
DeA-10140	380	<b>4641±54</b>	5282-5484	bulk peat
DeA-8347	400	<b>4638±26</b>	5372-5463	bulk peat
DeA-10141	500	<b>5949±36</b>	6677-6861	bulk peat
DeA-10142	600	<b>6989±43</b>	7785-7867	bulk peat
DeA-8348	700	<b>7909±33</b>	8600-8793	bulk peat
DeA-10143	800	<b>8687±45</b>	9539-9778	bulk peat
DeA-8349	900	<b>9273±36</b>	10369-10571	bulk peat

905  
 906  
 907  
 908  
 909  
 910  
 911  
 912  
 913  
 914  
 915  
 916  
 917  
 918  
 919  
 920  
 921  
 922  
 923



924 **Table 2: Ti-K correlation ( $R^2$ ), alongside average cps for K and Ti for each of the dust events as identified within the**  
 925 **Mohos core.**

<b>Dust Event</b>	<b>D1</b>	<b>D2</b>	<b>D3</b>	<b>D4</b>	<b>D5</b>	<b>D6</b>	<b>D7</b>	<b>D8</b>	<b>D9</b>	<b>D10</b>
<b>Ti-K Correlation (<math>R^2</math>)</b>	0.09	0.00	0.37	0.08	0.33	0.82	0.23	0.77	0.62	0.63
	106.5	106.4	121.5	106.1	193.0	431.8	308.4	268.0	197.0	288.6
<b>Average Ti (cps)</b>	1	1	1	9	6	0	4	4	7	8
<b>Average K (cps)</b>	48.68	57.80	52.33	32.05	63.14	124.3	108.2	76.04	67.71	349.8

926